LBL-14769
Preprint c.2

Lawrence Berkeley Laboratory
UNIVERSITY OF CALIFORNIA

Physics, Computer Science & Mathematics Division

Submitted for publication

PORTRAITS OF THE FLUX TUBE IN QED_3: A MONTE-CARLO SIMULATION WITH EXTERNAL SOURCES

T. Sterling and J. Greensite

RECEIVED
LAWRENCE
BERKELEY LABORATORY

NOV 10 1982

LIBRARY AND
DOCUMENTS SECTION

August 1982

Prepared for the U.S. Department of Energy under Contract DE-AC03-76SF00098

LBL-14769 c.2

DISCLAIMER

This document was prepared as an account of work sponsored by the United States Government. While this document is believed to contain correct information, neither the United States Government nor any agency thereof, nor the Regents of the University of California, nor any of their employees, makes any warranty, express or implied, or assumes any legal responsibility for the accuracy, completeness, or usefulness of any information, apparatus, product, or process disclosed, or represents that its use would not infringe privately owned rights. Reference herein to any specific commercial product, process, or service by its trade name, trademark, manufacturer, or otherwise, does not necessarily constitute or imply its endorsement, recommendation, or favoring by the United States Government or any agency thereof, or the Regents of the University of California. The views and opinions of authors expressed herein do not necessarily state or reflect those of the United States Government or any agency thereof or the Regents of the University of California.

August 1982 LBL-14769

PORTRAITS OF THE FLUX TUBE IN QED_3: A MONTE-CARLO SIMULATION WITH EXTERNAL SOURCES*

T. Sterling
Lawrence Berkeley Laboratory
University of California
Berkeley, CA 94720

and

J. Greensite†
Physics Department
University of California
Berkeley, CA 94720

ABSTRACT

We determine numerically, and display graphically, the electromagnetic energy distribution due to static sources in compact QED_3. Using the polymer formulation of the functional integral, Monte-Carlo simulations are performed with external sources included in the lattice action. Both the Wilson and Villain forms of the action are studied, and the string tension is determined in a small range of weak couplings. Our values for the string tension σ agree with previous Monte-Carlo studies using standard methods, but are not in good agreement with Polyakov's formulas in the range of couplings studied.

* This work was supported by the Director, Office of Energy Research, Office of High Energy and Nuclear Physics, Division of High Energy Physics of the U.S. Department of Energy under Contract DE-AC03-76SF00098.

† Participating guest at Lawrence Berkeley Laboratory.

I. INTRODUCTION

Computer simulations of lattice QCD have provided the best evidence so far of the coexistence of confinement and asymptotic freedom,[1] and recently there have even been efforts to extract the hadron spectrum from Monte-Carlo calculations.[2] Because of the importance of the Monte-Carlo method in gauge theory, it is appropriate to test the validity of this technique in as many ways as possible. In this paper we will carry out a Monte-Carlo simulation of compact QCD_3 with external sources included as part of the action. Our motivations are, first, to check whether the standard Monte-Carlo method might be missing configurations which are important to flux-tube formation, second, to measure the string-tension at much larger charge separations than have been used previously; and third, to generate (with the help of computer graphics) pictures of the electromagnetic energy distribution in confining flux-tubes.

Recall that the basic idea of the standard Monte-Carlo method, when applied to evaluating a VEV

$$\langle Q \rangle = \frac{\int \prod_\ell dU_\ell \, Q(U) e^S}{\int \prod_\ell dU_\ell \, e^S} \tag{1.1}$$

in lattice gauge theory, is to generate a sequence of "equilibrium" configurations $\{U_\ell^{eq}(m)\}$, where ℓ indexs links, and m indexs the mth equilibrium configuration in the sequence. These configurations, which represent an optimum balance between energy and entropy, should be typical of the most important vacuum gauge field configurations contributing to the partition function

$$Z = \int \prod_{\ell} dU_{\ell} e^{S}. \tag{1.2}$$

The VEV $\langle Q \rangle$ is then taken to be the average value of Q in a finite set of equilibrium configurations

$$\langle Q \rangle = \frac{1}{M} \sum_{m=1}^{M} Q[U_{\ell}^{eq}(m)]. \tag{1.3}$$

But one can now ask the question of whether, by generating vacuum configurations which are important in the denominator of (1.1), it is possible to completely miss the most important configurations contributing to the numerator of (1.1).

To illustrate the problem we have in mind, compare the monopole confinement mechanism analyzed by Polyakov in compact QED_3,[3] with the "spaghetti" vacuum picture advocated by the Copenhagen group (see, e.g., Ref. [4] and references therein). The former mechanism is an example of what we will call an "active" confinement scenario, and the latter is a "passive" scenario. In both pictures the vacuum is dominated by a special class of configurations, which are monopoles in one case and Z_N fluxons in the other (Fig. 1). The distinction between active and passive refers to the way that these configurations induce an area law suppression of large Wilson loops W(c). In the Polyakov model, monopole-antimonopole pairs tend to line up along the minimal area of the loop, and this magnetic screening effect on the surface of the loop gives rise to an area law $W(c) \sim \exp[-\mu S_{min}]$. So the presence of the Wilson loop affects the relevant field configurations, and the numerator in (1.1) should be dominated by screening

configurations as shown in Fig. 2(a). On the other hand, in the spaghetti vacuum picture, the Wilson loop gets an area suppression simply through random fluctuations in the number of Z_N fluxons penetrating the surface, as in Fig. 2(b). The relevant configurations in the numerator and denominator are exactly the same. So the distinction between "active" and "passive" confinement scenarios depends on whether the Wilson loop is viewed as part of the action, thereby "actively" determining the relevant field configurations, or instead as a passive counter, to be averaged over equilibrium configurations determined by the source-free action.

The Monte-Carlo technique is naturally suited to the passive confinement scenario, but would it also give the correct result in an active confinement case? Since the standard algorithm generates field configurations with no reference to external sources, the configuration in Fig. 2(a) would be generated very infrequently. Of course, there is no question that the Monte-Carlo procedure, if continued indefinitely, would converge to the right answer for the Wilson loop. If the algorithm were to run indefinitely, eventually the whole phase space would be sampled. The real question is whether the relevant configurations, such as those in Fig. 2(a), are generated in a reasonable number of Monte-Carlo iterations.

In order to study this question, we have computed the string tension of compact QED in a non-standard way: that is, by a Monte-Carlo calculation of the electromagnetic energy due to external charges, which are included as part of the action. Since the field energy density inside a flux-tube is almost constant as the charges are separated, this technique allows us to compute the string tension

at large charge separations. Our computations have been done with charge separations of up to 16 lattice spacings, and there is no real barrier to doubling (or even quadrupling) that separation. This is in contrast to standard calculations where the string tension is extracted from the log of the Wilson loops, and where charge separations of about 8 lattice spacings seem to be the practical limit. This is because the value of a Wilson loop is exponentially suppressed as the area grows, and the string tension is lost in the noise.

In order to include external charges, and still have the action remain purely real (see next section), we have used the polymer form of the functional integral for numerical simulations. The procedure is essentially equivalent to a Monte-Carlo in the dual variables of the theory.[5] Using the Wilson form of the compact QED_3 lattice action, we have extracted the string tension in a small region $2 \leqslant \beta < 2.3$ of couplings. It is only in this small "window" of weak couplings that one may hope to detect a flux tube by Monte-Carlo methods.[6] Beyond $\beta = 2.3$, the width of the flux tube exceeds any practical lattice size.

The string tensions which we have extracted in this small region of couplings are in reasonable agreement with those computed by standard methods in Ref. [5,6]. Since string tensions obtained by the two methods agree, we conclude that the "active-vs.-passive" problem raised above does not pose any threat to the standard method.

We have also computed a string tension, using the Villain form of the lattice action, at $\beta_v = 1.6$, which is inside the weak-coupling region of the Villain action. This value can be compared directly

with Polyakov's analytical expression for the string tension. The agreement of the theoretical and "experimental" values is not very good; the values disagree by almost a factor of 2. The probable explanation of this disagreement is just that the saddlepoint approximation used to derive Polyakov's formula is not very accurate at $\beta_v = 1.6$.

Finally, we have generated (with the help of computer graphics) a series of pictures of the electromagnetic field intensities due to external sources. It is, of course, no surprise that the electromagnetic field energy in compact QED_3 is restricted to a tube of flux. But it is still of interest to have a graphical confirmation of this fact.

II. EXTERNAL SOURCES AND COMPUTER SIMULATIONS

The electromagnetic energy density $\tilde{\varepsilon}(x)$ due to a pair of static charges e^+e^- is given by

$$\tilde{\varepsilon}(x) = \langle e^+e^- \,|\, \frac{1}{2}\,(\underset{\sim}{E}^2(x) + B^2(x) \,|\, e^+e^- \rangle - \langle 0 \,|\, \frac{1}{2}(\underset{\sim}{E}^2 + B^2) \,|\, 0 \rangle, \tag{2.1}$$

where $|e^+e^- \rangle$ is the ground state of the photon field in the presence of external charges e^+e^-, and $|0\rangle$ is the ground state with no external charges. In the Euclidean, latticized version this expression becomes

$$\tilde{\varepsilon}(x) = (\varepsilon_E(x) - \varepsilon_B(x)) - (\varepsilon_E^0 - \varepsilon_B^0), \tag{2.2}$$

where, in 3 Euclidean dimensions

$$\varepsilon_E = \varepsilon_{E_1} + \varepsilon_{E_2},$$

$$\varepsilon_{E_i}(x) = \frac{\int \prod_\ell \frac{d\theta_\ell}{2\pi} \cos\theta_{p_{0i}(x)} W_1 W_2 e^{\beta\sum_p a_p}}{\int \prod_\ell \frac{d\theta_\ell}{2\pi} W_1 W_2 e^{\beta\sum_p a_p}}$$

$$\varepsilon_B(x) = \frac{\int \prod_\ell \frac{d\theta_\ell}{2\pi} \cos\theta_{p_{12}(x)} W_1 W_2 e^{\beta\sum_p a_p}}{\int \prod_\ell \frac{d\theta_\ell}{2\pi} W_1 W_2 e^{\beta\sum_p a_p}}$$

$$\varepsilon_{E_i}^0 = \varepsilon_B^0 = E_p = \frac{\int \prod_\ell \frac{d\theta_\ell}{2\pi} \cos\theta_p e^{\beta\sum_p a_p}}{\int \prod_\ell \frac{d\theta_\ell}{2\pi} e^{\beta\sum_p a_p}} \tag{2.3}$$

which correspond to electromagnetic energy densities in the weak-coupling limit. In our notation $p_{ij}(x)$ is a plaquette with corners at $\{x, x+\hat{i}, x+\hat{i}+\hat{j}, x+\hat{j}\}$ and θ_p is the lattice curl

$$\theta_{p_{ij}}(x) = \theta(x, x+\hat{i}) + \theta(x+\hat{i}, x+\hat{i}+\hat{j})$$

$$-\theta(x+\hat{j}, x+\hat{i}+\hat{j}) - \theta(x\ x+\hat{j}). \tag{2.4}$$

The Wilson lines W_1, W_2 are products of link variables on parallel lines L_1, L_2 which run through the periodic lattice in the time direction,

$$W_1 = \exp i[\theta(x_1, x_1+\hat{t}) + \theta(x_1+\hat{t}, x_1+2\hat{t}) + \ldots + \theta(x_1+(T-1)\hat{t}\ x_1+T\hat{t})]$$

$$W_2 = \exp -i[\theta(x_2, x_2+\hat{t}) + \theta(x_2+\hat{t}, x_2+2\hat{t}) + \ldots + \theta(x_2+(T-1)\hat{t}, x_2+T\hat{t})], \tag{2.5}$$

where x_1, x_2 are lattice sites at $t = 0$, and T is the extent of the periodic lattice in the time direction. Note that the difference in relative signs of ε_E and ε_B in (2.2) is a result of rotating from Minkowski to Euclidean space.

In order to carry out a numerical simulation of compact QED_3 with external sources, one would like to include the Wilson lines as part of the action, i.e.

$$\tilde{a} = \beta\sum_p a_p + \ln W_1 + \ln W_2, \tag{2.6}$$

and then apply the standard Metropolis or heat-bath algorithms to $\tilde{a}$ rather than a_p. But this method won't work. The problem is that

since the Wilson lines are not positive definite, $\tilde{a}$ as defined above is not necessarily real, and the standard algorithms cannot be applied. So we turn instead to the polymer formulation of the gauge theory.

Let us first write the source-free functional integral in polymer form. Begin with functional integral

$$Z = \int \prod_{\ell} \frac{d\theta_\ell}{2\pi} \; e^{\beta \sum_p a_p}, \tag{2.7}$$

and expand the lattice action in characters

$$e^{a_p(\theta_p)} = A(\beta)[1 + \sum_{r_p} B_{r_p}(\beta) e^{ir_p\theta_p}], \tag{2.8}$$

where, for the Wilson action

$$A(\beta) = I_0(\beta),$$

$$B_r(\beta) = I_r(\beta)/I_0(\beta), \tag{2.9}$$

and, for the Villain action

$$A(\beta) = e^{\beta}/\sqrt{2\pi\beta},$$

$$B_r(\beta) = e^{-r^2/2\beta} \tag{2.10}$$

The sum in (2.8) is over all positive and negative integers, excluding the trivial representation $r_p = 0$. Substituting (2.8) into (2.7) and integrating over link variables θ_ℓ yields

$$Z = A^{N_p} \sum_{\substack{\text{polymers} \\ Q}} \sum_{\substack{r_p \\ p\varepsilon Q}} e^{\sum_n [\log B_n(\beta)] \cdot S_n} \prod_{\ell\varepsilon Q} \delta_\ell(\text{constraint}) \tag{2.11}$$

where:

N_p = total no. of plaquettes on the lattice

Q = closed, but not necessarily connected, surfaces on the lattice (polymers)

S_n = no. of plaquettes in polymer Q with "flux" (group representation) $r_p = n$.

So the sum is over surfaces Q and over flux covering each surface r_p ($p\varepsilon Q$) with the flux subject to a certain constraint: Each link $\ell\varepsilon Q$ is connected (in 3 dimensions) to four plaquettes $p_1(\ell)$, $p_2(\ell)$, $p_3(\ell)$, $p_4(\ell)$ (ordered 1-4 in a clockwise direction around the link). Denote the flux associated with these plaquettes $r[p_1(\ell)]$, $r[p_2(\ell)]$, etc., with $r[p(\ell)] = 0$ if plaquette $p_i(\ell)$ does not belong to Q. The Kronecker-delta constraint in (2.11) is just

$$\delta_\ell(\text{constraint}) = \delta_{\{r[p_1(\ell)+r[p_2(\ell)]-r[p_3(\ell)]-r[p_4(\ell)]\},\, 0}. \tag{2.12}$$

The form (2.11) of Z is suitable for Monte-Carlo calculations, using

$$a[Q, \{r_p\}] = \sum_n [\log B_n(\beta)] S_n \tag{2.13}$$

for the action. In this case, the geometry of the polymer Q and the plaquette flux $\{r_p\}$ are the variables which must be generated by the Monte-Carlo algorithm, subject to the constraint (2.12). Of course, this constraint could be eliminated by carrying out the Monte-Carlo calculation in the spin system corresponding to the dual theory.[5] However, since we have other applications in mind for polymer simulations (see the last section of Ref. [7]), we will continue to use

the polymer formulation of the U(1) theory.

We now describe our Monte-Carlo algorithm for Eq. (2.11). In 3 dimensions each site on the dual lattice is centered inside a cube of plaquettes. The procedure is to sweep through the sites of the dual lattice, and at each dual site operate simultaneously on the corresponding cube of plaquettes (labeled as in Fig. 3). There are three possible operations:

A) add a cube of minimal flux to an existing polymer or vacuum

$$r[p_1] = r[p_1] + 1,\ r[p_2] = r[p_2] + 1,\ r[p_3] = r[p_3] + 1$$

$$r[p_4] = r[p_4] - 1,\ r[p_5] = r[p_5] - 1,\ r[p_6] = r[p_6] - 1,$$

B) add an "anticube" of minimal flux to an existing polymer or vacuum

$$r[p_1] = r[p_1] - 1,\ r[p_2] = r[p_2] - 1,\ r[p_3] = r[p_3] - 1$$

$$r[p_4] = r[p_4] + 1,\ r[p_5] = r[p_5] + 1,\ r[p_6] = r[p_6] + 1,$$

C) do nothing.

Operations (A) and (B), acting on vacuum, create cubes and "anti-cubes" of minimal flux. When these operations act on existing polymers, they modify or destroy them. It is easy to see that any polymer generated by succesive operations of types (A) and (B) will automatically satisfy the constraint (2.12). We can now follow the usual Monte-Carlo procedure by sweeping through all the dual sites of the lattice, and at each site use the Metropolis algorithm to determine which of the operations (A), (B), or (C) is to be applied. In this way we have computed the plaquette energy as a function of β

$$\varepsilon^0 = \frac{1}{N_p}\frac{\partial}{\partial\beta}\ \ln Z = \frac{1}{A}\frac{\partial A}{\partial\beta} + \frac{1}{N_p}\sum_n \frac{1}{B_n}\frac{\partial B_n}{\partial\beta} < S_n > , \qquad (2.14)$$

and checked that these values agree with values obtained by the standard method (i.e. Monte-Carlo algorithm applied to link variables).

The inclusion of static charges modifies (2.7) to

$$Z_{e^+e^-} = \int \prod_\ell \frac{d\theta_\ell}{2\pi}\ W_1 W_2 e^{\beta\sum_p a_p}, \qquad (2.15)$$

which becomes, following the previous steps

$$Z_{e^+e^-} = A^{N_p} \sum_{\substack{\text{polymers}\\ Q_{12}}} \sum_{\substack{r_p\\ p\varepsilon Q_{12}}} e^{\sum_n [\log B_n(\beta)]\cdot S_n}$$

$$\cdot \prod_{\substack{\ell\varepsilon Q_{12}\\ \ell\notin L_1 L_2}} \delta\{r[p_1(\ell)]+r[p_2(\ell)]-r[p_3(\ell)]-r[p_4(\ell)]\},\ 0$$

$$\cdot \prod_{\ell\varepsilon L_1} \delta\{r[p_1(\ell)]+r[p_2(\ell)]-r[p_3(\ell)]-r[p_4(\ell)]\},-1$$

$$\cdot \prod_{\ell\varepsilon L_2} \delta\{r[p_1(\ell)]+r[p_2(\ell)]-r[p_3(\ell)]-r[p_4(\ell)]\},1, \qquad (2.16)$$

where L_1, L_2 are the Wilson lines, and $\{Q_{12}\}$ is the set of all those polymers which (to satisfy all the constraints) must include a surface bounded by L_1, L_2. Note that the external charges are included simply by the constraints, while the action is unchanged.

The new constraints on flux around lines L_1, L_2 are most easily satisfied by incorporating them into the initialization of the lattice, and using the same "change-a-cube" algorithm as before. That is, instead of a simple cold-start, which is just setting all $r_p = 0$,

choose any planar surface bounded by L_1 and L_2 (such as the minimal surface) and set $r_p = 1$ on all plaquettes along that surface. With this initial condition, polymers generated by the change-a-cube method automatically satisfy the new constraints. With this technique we can now compute VEVs (denoted $\langle\ \rangle_{e^+e^-}$) in compact QED_3 with external sources.

We will be interested especially in the energy densities (2.3), which are, for the Wilson action

$$\tilde{\varepsilon}_{E_k}(x) = \frac{I_1(\beta)}{I_0(\beta)} + \sum_{n\neq 0}\left[\frac{I_{n+1}+I_{n-1}}{2I_n} - \frac{I_1}{I_0}\right]\langle\delta_{r[p_{ok}(x)],n}\rangle_{e^+e^-} - E^p ,$$

$$\tilde{\varepsilon}_B(x) = \frac{I_1(\beta)}{I_0(\beta)} + \sum_{n\neq 0}\left[\frac{I_{n+1}+I_{n-1}}{2I_n} - \frac{I_1}{I_0}\right]\langle\delta_{r[p_{12}(x)],n}\rangle_{e^+e^-} - E^p , \tag{2.17}$$

$$E_p = \frac{I_1(\beta)}{I_0(\beta)} + \frac{1}{N_p}\sum_{n\neq 0}\left[\frac{I_{n+1}+I_{n-1}}{2I_n} - \frac{I_1}{I_0}\right]\langle S_n\rangle ,$$

and for the Villain action

$$\tilde{\varepsilon}_{E_K}(x) = 1 - \frac{1}{2\beta} + \sum_{n\neq 0}\frac{n^2}{2\beta^2}\langle\delta_{r[p_{ok}(x)],n}\rangle_{e^+e^-} - E_p$$

$$\tilde{\varepsilon}_B(x) = 1 - \frac{1}{2\beta} + \sum_{n\neq 0}\frac{n^2}{2\beta^2}\langle\delta_{r[p_{12}(x)],n}\rangle_{e^+e^-} - E_p$$

$$E_p = 1 - \frac{1}{2\beta} + \frac{1}{N_p}\sum_n\frac{n^2}{2\beta^2}\langle S_n\rangle . \tag{2.18}$$

Since the Wilson lines run through the periodic lattice in the time-like direction, we can improve our statistics by time-averaging, i.e.

$$\tilde{\varepsilon}(\underset{\sim}{x}) = \frac{1}{T}\sum_t \tilde{\varepsilon}(\underset{\sim}{x}, t) \tag{2.19}$$

where T is the number of links on the lattice in the timelike direction.

III. RESULTS

The Wilson lines L_1, L_2 are separated by 16 lattice spacings in the $\hat{x}$ direction, and we define

$$\tilde{\varepsilon}_{E_{||}}(\underset{\sim}{x}) = \tilde{\varepsilon}_{E_1}(\underset{\sim}{x}),$$

$$\tilde{\varepsilon}_{E_\perp}(\underset{\sim}{x}) = \tilde{\varepsilon}_{E_2}(\underset{\sim}{x}), \tag{3.1}$$

to be the (time-averaged) energy densities due to electric fields which are parallel ($E_{||}$) or perpendicular ($E_\perp$) to the x-axis. The total energy density is

$$\tilde{\varepsilon}(\underset{\sim}{x}) = \tilde{\varepsilon}_{E_{||}}(\underset{\sim}{x}) + \tilde{\varepsilon}_{E_\perp}(\underset{\sim}{x}) - \tilde{\varepsilon}_B(\underset{\sim}{x}). \tag{3.2}$$

Now it is well known that the electromagnetic energy density due to external charges should be concentrated in a flux-tube in compact QED_3, and the string tension σ is simply the energy/unit length of the flux tube. We need to evaluate σ at weak couplings, where $\tilde{\varepsilon}(x)$ in (3.2) corresponds to the Hamiltonian energy density, and σ can be compared with the string tensions found by standard Monte-Carlo. However, as shown in Ref. [6], there is only a small "window" of couplings $\beta \sim 2.0$-2.3 where it may be possible to extract a string tension. We have therefore concentrated our Monte-Carlo efforts in this range, and the results are shown in Fig. 4-7. Figure 4 shows the distribution of total energy density $\tilde{\varepsilon}$, while Fig. 5-7 break this density into component electric and magnetic pieces.

The figures show very clearly the presence of a confining flux tube. The tube is quite narrow and well-defined at $\beta = 1.8$, which is just within the strong-coupling regime. As β is increased the field intensities drop and the tube width broadens, until at $\beta = 2.3$ the flux tube can just barely be distinguished above the background. In the graphical display, time-averaged energy-densities in the x-y plane associated with plaquettes $p_{ij}(\underset{\sim}{x}, t)$ have been mapped into surfaces. The height of the surface at site $\underset{\sim}{x}$ represents the value of $\tilde{\varepsilon}_{E_{||}}(\underset{\sim}{x})$, $\tilde{\varepsilon}_{E_\perp}(\underset{\sim}{x})$ or $\tilde{\varepsilon}_B(\underset{\sim}{x})$. In the case of the total energy density $\tilde{\varepsilon}$, we have averaged the $\tilde{\varepsilon}_{E_{||}}$ components, i.e.

$$\tilde{\varepsilon}(x) = \frac{1}{2}[\tilde{\varepsilon}_{E_{||}}(\underset{\sim}{x}) + \tilde{\varepsilon}_{E_{||}}(\underset{\sim}{x} + \hat{j})] + \tilde{\varepsilon}_{E_\perp}(\underset{\sim}{x}) - \tilde{\varepsilon}_B(\underset{\sim}{x}). \tag{3.3}$$

This averaging was done to avoid an artificial asymmetry in the total energy density, which would occur when adding electric and magnetic field energies because of the convention of associating plaquettes $p_{ij}(x)$ with sites $\underset{\sim}{x}$. Using the definition (3.3), the total energy density is symmetric in the y-direction across the flux tube.

A few words about the computer simulations are in order. The calculations were performed on CDC 6600 and 7600 computers, and as many as 75000 iterations were used to produce the values of $\tilde{\varepsilon}$ shown here. Convergence was checked by comparing runs with hot and cold starts. A cold start sets all $r_p = 0$ except on the minimal surface. A hot start begins with a cold start initialization, and proceeds with 50 iterations at $\beta = 50$. Then β is reset to the proper value, and the iteration continues. Note that for the polymer simulations

(which is essentially equivalent to a Monte-Carlo simulation in dual variables),[5] a "cold" start corresponds to $\beta = 0$, and a "hot" start corresponds to $\beta \gg 1$.

The lattice size is 16 (t-direction) × 16 (y-direction) × 24 (x-direction). Since the periodic lattice is only 24 spacings in the in the x-direction, one might wonder why the flux tube is 16 spacings long, rather than the 8 lattice spacings which, due to the periodicity of the lattice, is the actual minimal distance between the charges. The answer lies in the initialization procedure, where the flux tube is set to lie along the x-axis in the "long" (16 spacings) distance between the charges. Quantum fluctuations thicken the tube, as they would in an infinite lattice, but are incapable of actually flipping the tube into the "short" (8 spacings) direction. In fact, such a flip could only occur by operating simultaneously on a sheet of plaquettes running across the entire periodic lattice, and this non-local operation is not included in the change-a-cube algorithm. The consequence is that a flux tube can only lie along one, rather than two, lines joining the two charges, which is, of course, the case in an infinite volume. The algorithm thereby eliminates a distortion in the field distribution due to the periodicity of the lattice. A further virtue is that our initialization has allowed us to use an undersized lattice in the x-direction, which allows some economy in computer time. We have checked that our results are not sensitive to an increase in lattice size.

With the data shown in Fig. 4, we have extracted a string tension σ by measuring the energy density/unit length in the center of the flux tube, thereby eliminating the Coulombic contribution which is large near the static sources. Our values for σ are shown in Fig.8, and compared with the values obtained by a standard Monte-Carlo in Ref. [6], where σ is extracted from the log of the Wilson loops. The two sets of values seem to be in reasonably good agreement.

Polykov has derived a formula for the string tension in 3-dimensional compact U(1) theory,[3] and this work has been extended by Banks, Myerson, and Kogut[8] to lattice QED_3 with a Villain action. Polyakovs formula in the lattice theory is

$$\sigma = \frac{4\sqrt{2}}{\pi\sqrt{\beta}}\, e^{-\pi^2 V(0)\beta} \tag{3.4}$$

where σ has been scaled by the lattice spacing^2 and is dimensionless, and $V(0) = .2527$ is a constant associated with the lattice Coulomb propagator. We cannot directly compare (3.4) with the string tensions in Fig. 8. Eq. (3.3) was derived for the Villain action, and there are substantial differences between the Wilson and Villain actions in $2.0 \leqslant \beta \leqslant 2.3$ range. So instead we have performed a separate Monte-Carlo run using the Villain action at $\beta_v = 1.6$. The energy distribution at this value of β is shown in Fig. 9, and we find that

$$\sigma_{\text{Monte-Carlo}} = .016 \ , \tag{3.5}$$

compared to the value obtained from (3.4)

$$\sigma_{\text{Polyakov}} = .026 \,, \tag{3.6}$$

at $\beta_v = 1.6$. The agreement between the Monte-Carlo value and the theoretical prediction for σ is not very good, but we do not feel that this is cause for concern. Polyakov's formula is based on a saddlepoint approximation which is only accurate as $\beta_v \to \infty$. The difference between (3.5) and (3.6) only means that, at the weakest couplings where we can obtain a string tension by numerical simulations, the saddlepoint approximation is not very accurate. We think it is not possible, in this small range of β, to demonstrate the expoential dependence of σ on β [6].

IV. CONCLUSIONS

Our main conclusion is that the string-tension extracted from a Monte-Carlo simulation including external sources in the action agrees with string tensions extracted by the standard methods. This means that the possible objection to the standard method which was raised in the introduction, namely, that the standard method might miss relevant configurations in an "active" confinement scenario, seems to be unfounded. We have also shown graphically that electromagnetic energy is confined to flux tubes in compact QED_3, a fact which has long been understood on theoretical grounds.

There may be other applications for polymer simulations by the change-a-cube method outlined here. For example, the method could be adapted to computing the entropy of self-avoiding planar surfaces, as outlined in Ref. [7]. The idea is to simulate random surface fluctuations of self-avoiding planar surfaces Q, using a Boltzman factor $\exp[-\beta\,\text{Area}\,(Q)]$. One would then compute $\langle \text{Area} \rangle$ as a function of β, and the entropy of planar surfaces ($\sim e^{\varepsilon S}$) could be identified at the point $\beta = \beta_c = \varepsilon$ where $\langle \text{Area} \rangle \to \infty$. The entropy factor ε may be relevant in determing the upper critical dimension for confinement at weak couplings [7].

It would be interesting to extend the method used here to non-abelian theories, since it would allow the determination of σ at much larger lattice separations than have been used so far. Unfortunately, the polymer action for a non-abelian theory is very complicated and probably not applicable to Monte-Carlo calculations.

ACKNOWLEDGMENT

This work was supported by the Director, Office of Energy Research, Office of High Energy and Nuclear Physics, Division of High Energy Physics of the U.S. Department of Energy under Contract DE-AC03-76SF00098.

REFERENCES

[1]. M. Creutz, Phys. Rev. D23, (1981) 1815.

[2]. H. Hamber and G. Parisi, Phys. Rev. Lett. 47 (1981) 1972; D. Weingarten, Phys. Lett. 109B, (1982) 57.

[3]. A. Polyakov, Nucl. Phys. B120, (1977) 429.

[4]. J. Ambjørn and P. Olesen, Nucl. Phys. B170, [FS1] (1980) 265.

[5]. G. Bhanot and M. Creutz, Phys. Rev. D21, (1980) 2892.

[6]. J. Ambjørn, A. J. G. Hey, S. Otto, String Tensions for Lattice Gauge Theories in 2 + 1 Dimensions, CalTech preprint CALT-68-902 (March 1982).

[7]. K. Bardakci and J. Greensite, Summing Bubbling Surfaces, Berkeley preprint UCB-PTH-82/9 (June 1982).

[8]. T. Banks, R. Myerson, and J. Kogut, Nucl. Phys. B129, (1977) 493.

FIGURE CAPTIONS

[Figure 1]. Vacuum configurations with no external sources: (a) monopole plasma in compact QED_3; (b) QCD "spaghetti" vacuum.

[Figure 2]. Vacuum configurations with a Wilson loop source: (a) monopole plasma; (b) "spaghetti" vacuum.

[Figure 3]. Convention for labeling plaquettes on a cube.

[Figure 4]. Total electromagnetic energy density due to external charges 16 lattice spacings apart. Energy distribution at $1.8 \leqslant \beta \leqslant 2.3$ is shown in (a) - (e).

[Figure 5]. Breakdown of the energy density into components $\tilde{\varepsilon}_{E_{||}}$, $\tilde{\varepsilon}_{E_{\perp}}$, $\tilde{\varepsilon}_B$ at $\beta = 1.8$.

[Figure 6]. Energy density components at $\beta = 2.1$.

[Figure 7]. Energy density components at $\beta = 2.3$.

[Figure 8]. Values of σ in the range $2.0 \leqslant \beta \leqslant 2.3$. Solid dots are our values, with errors estimated to be about 5%. Open circles are values for σ obtained by standard methods in Ref. [6].

[Figure 9]. Energy distribution for the Villain action at $\beta_v = 1.6$. (a) total energy $\tilde{\varepsilon}$; (b) $\tilde{\varepsilon}_{E_{||}}$, (c) $\tilde{\varepsilon}_{E_{\perp}}$; (d) $\tilde{\varepsilon}_B$.

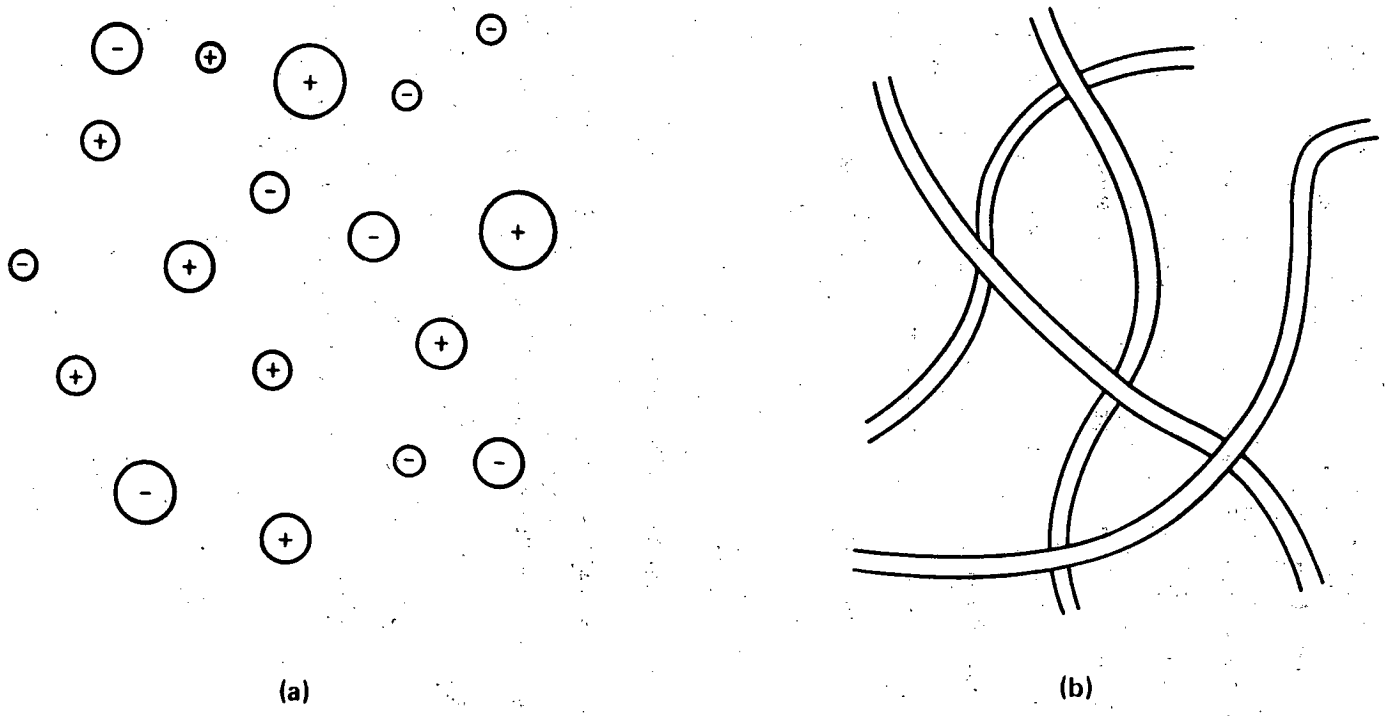

FIGURE 1

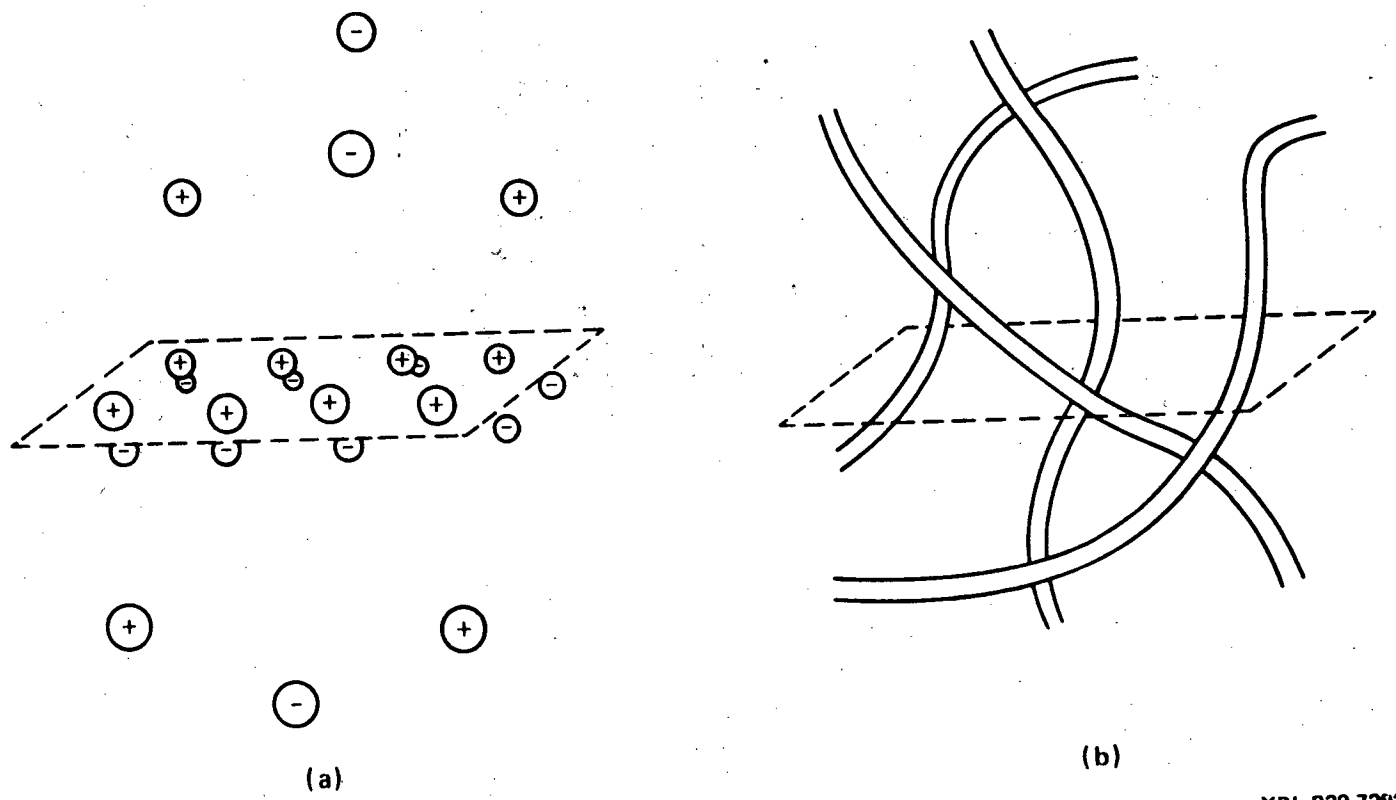

XBL-829-7292

FIGURE 2

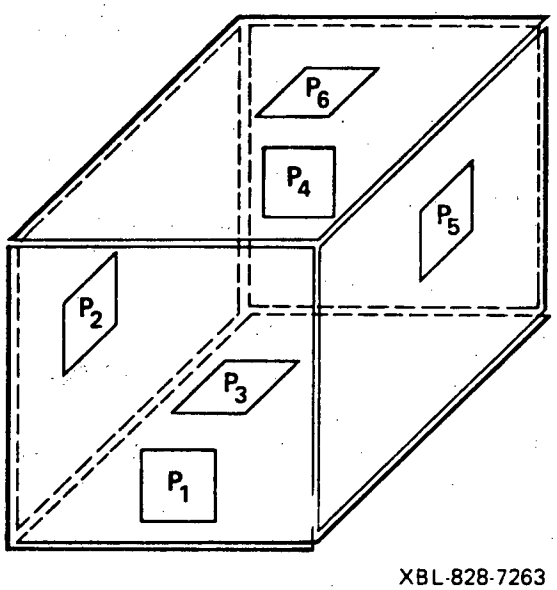

FIGURE 3

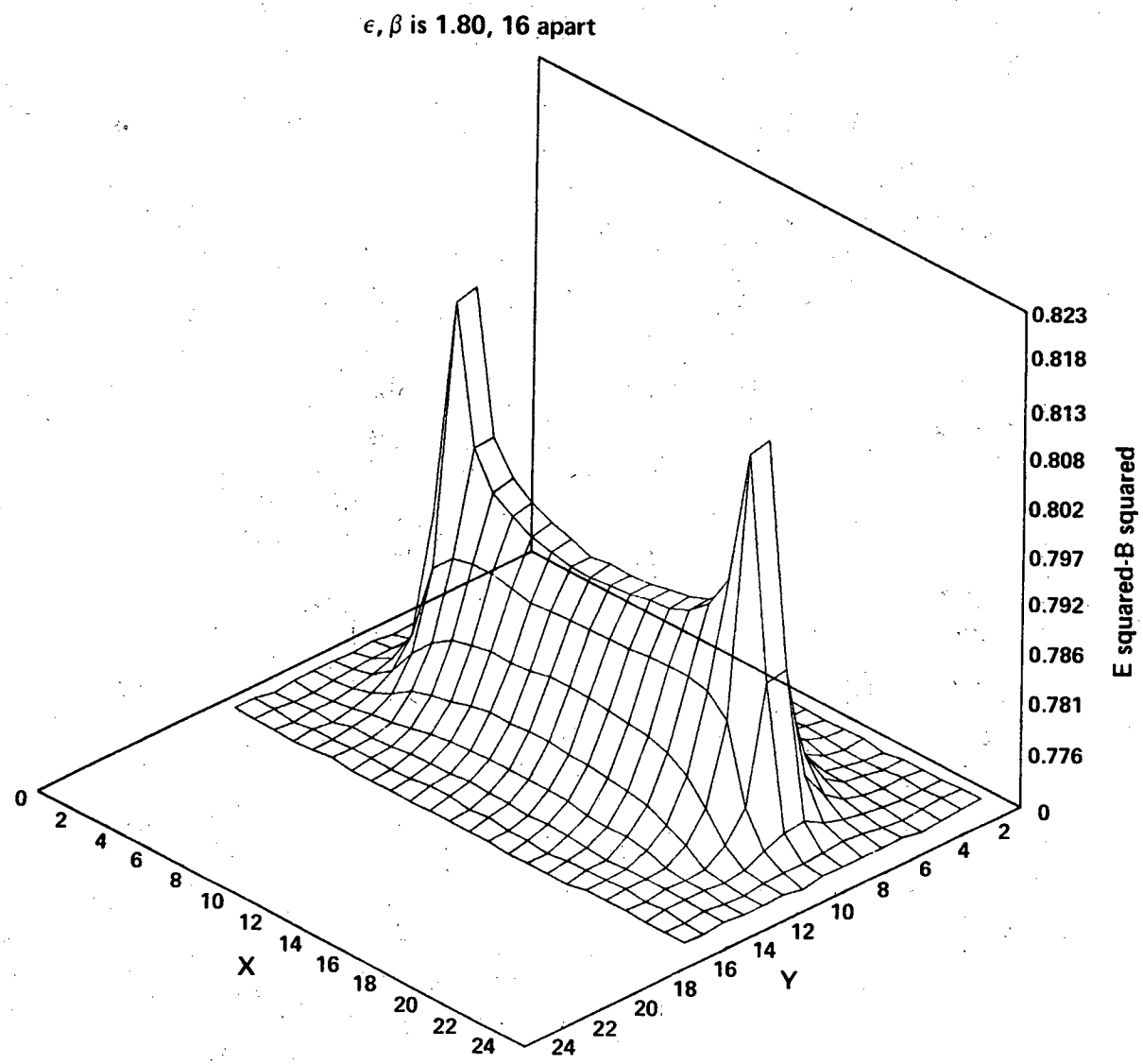

FIGURE 4A

XBL-829-7282

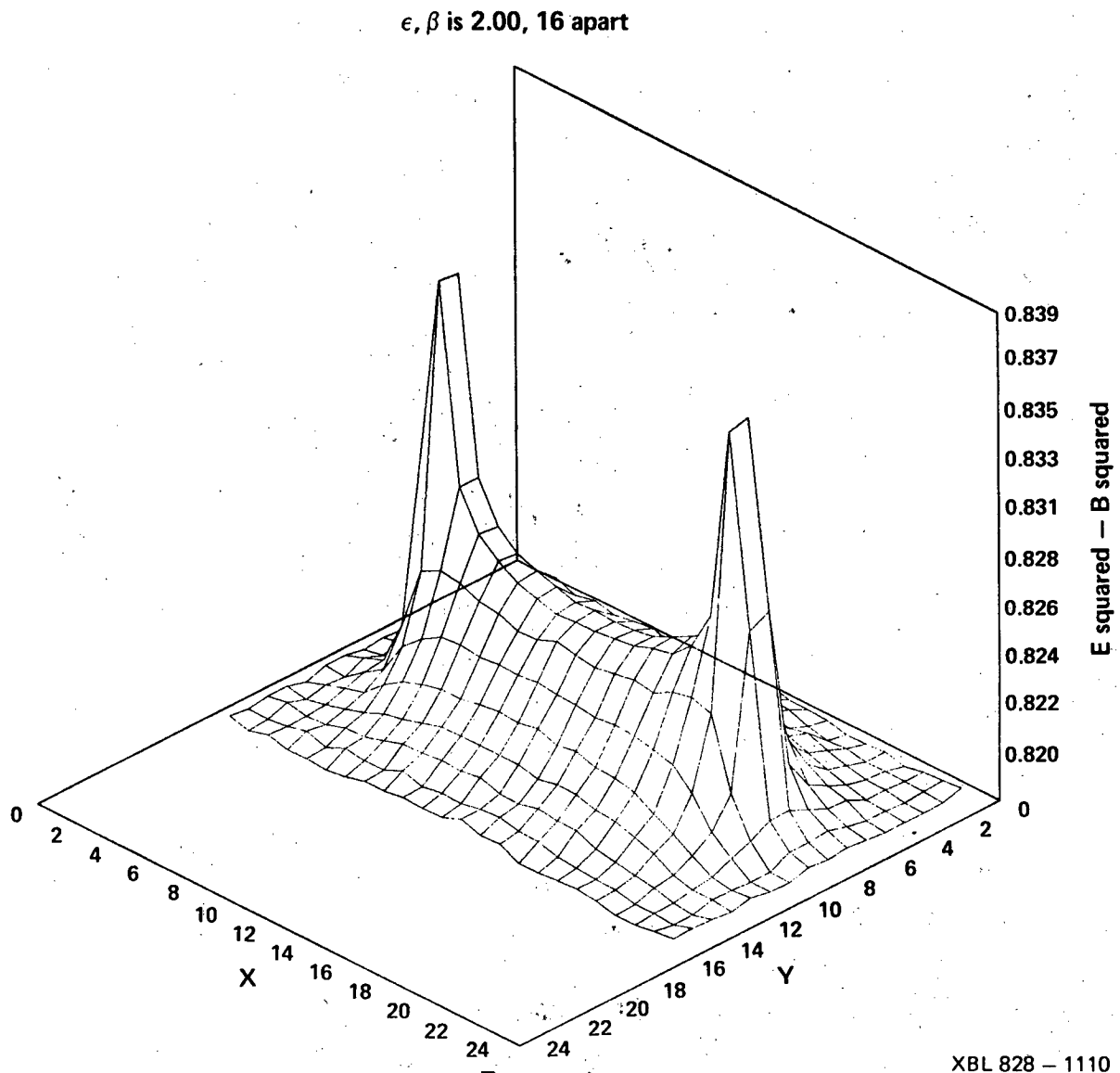

XBL 828 – 1110

FIGURE 4B

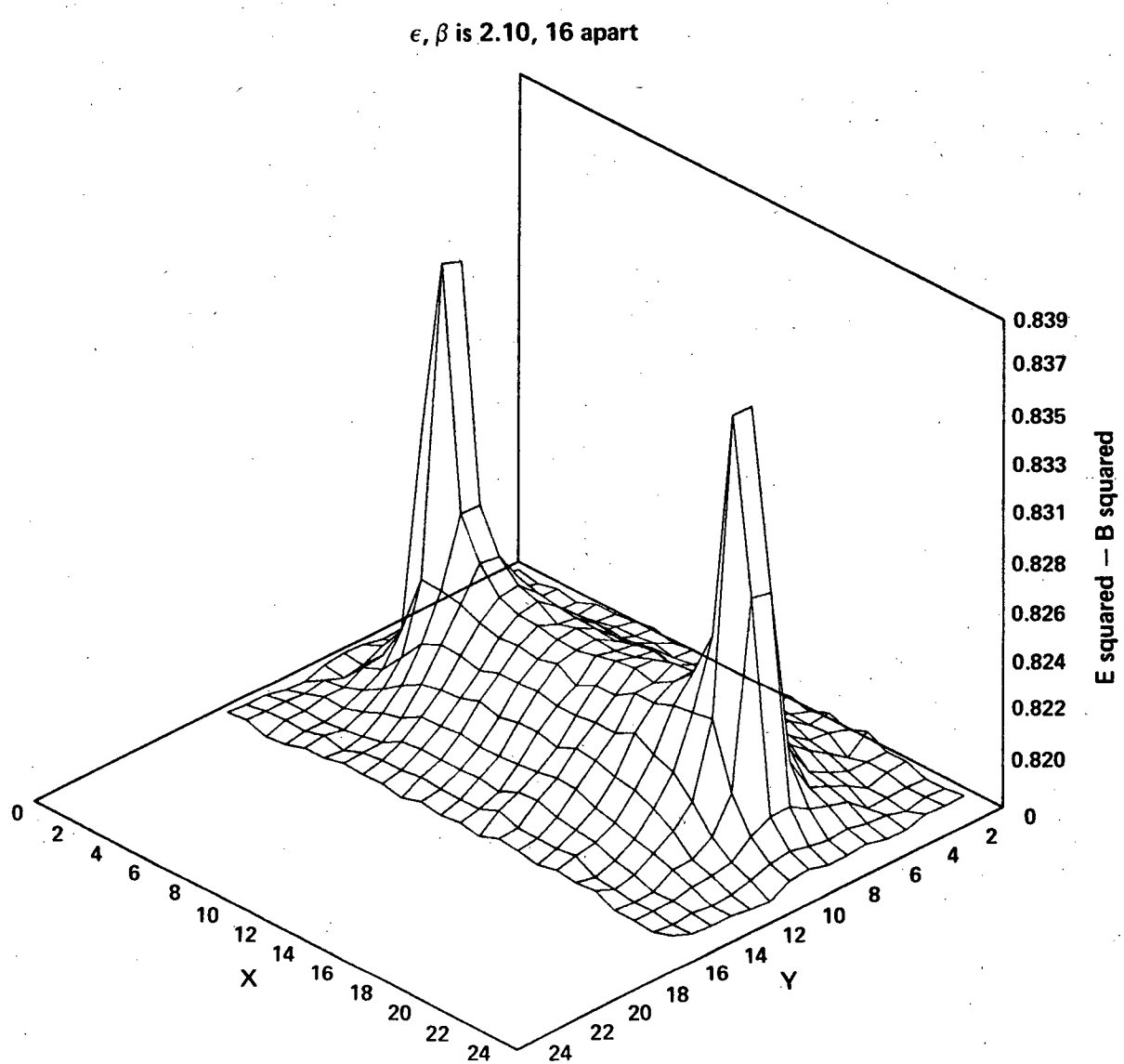
ε, β is 2.10, 16 apart
0.839
0.837
0.835
0.833
0.831
0.828
0.826
0.824
0.822
0.820
0
E squared — B squared
0
2
4
6
8
10
12
14
16
18
20
22
24
X
Y
XBL-829-7299

FIGURE 4C

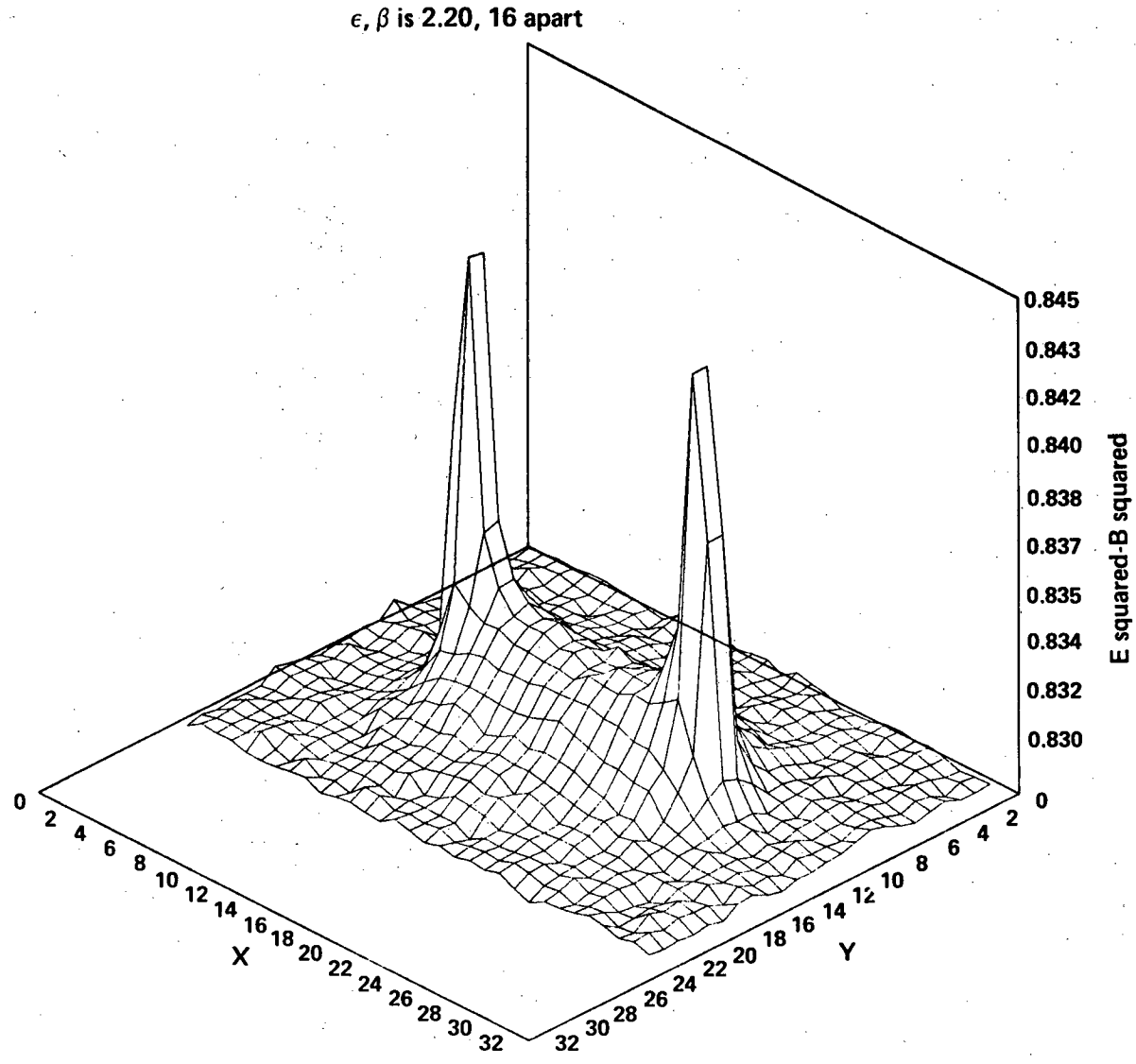

XBL-829-7284

FIGURE 4D

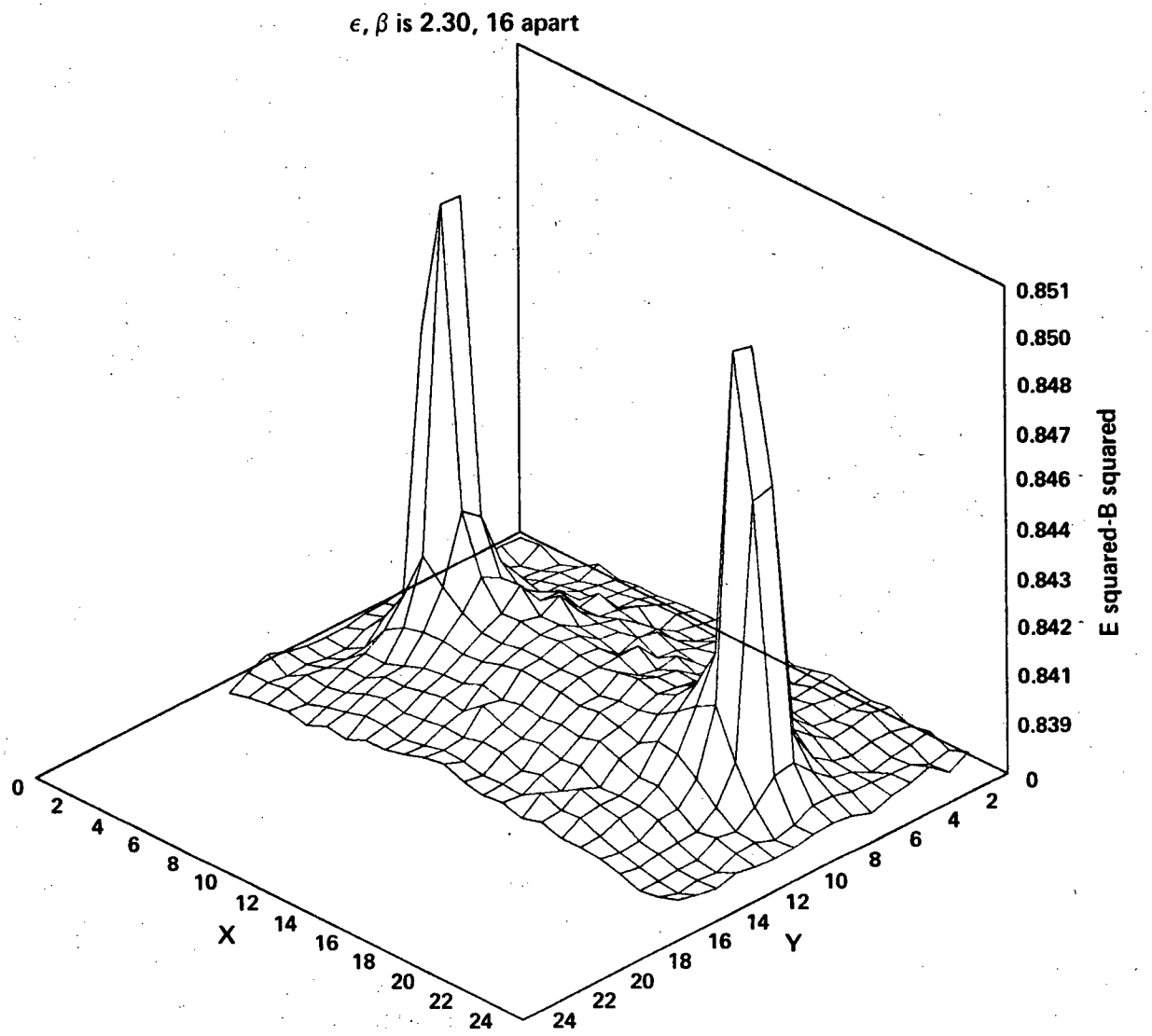

XBL-829-7283

FIGURE 4E

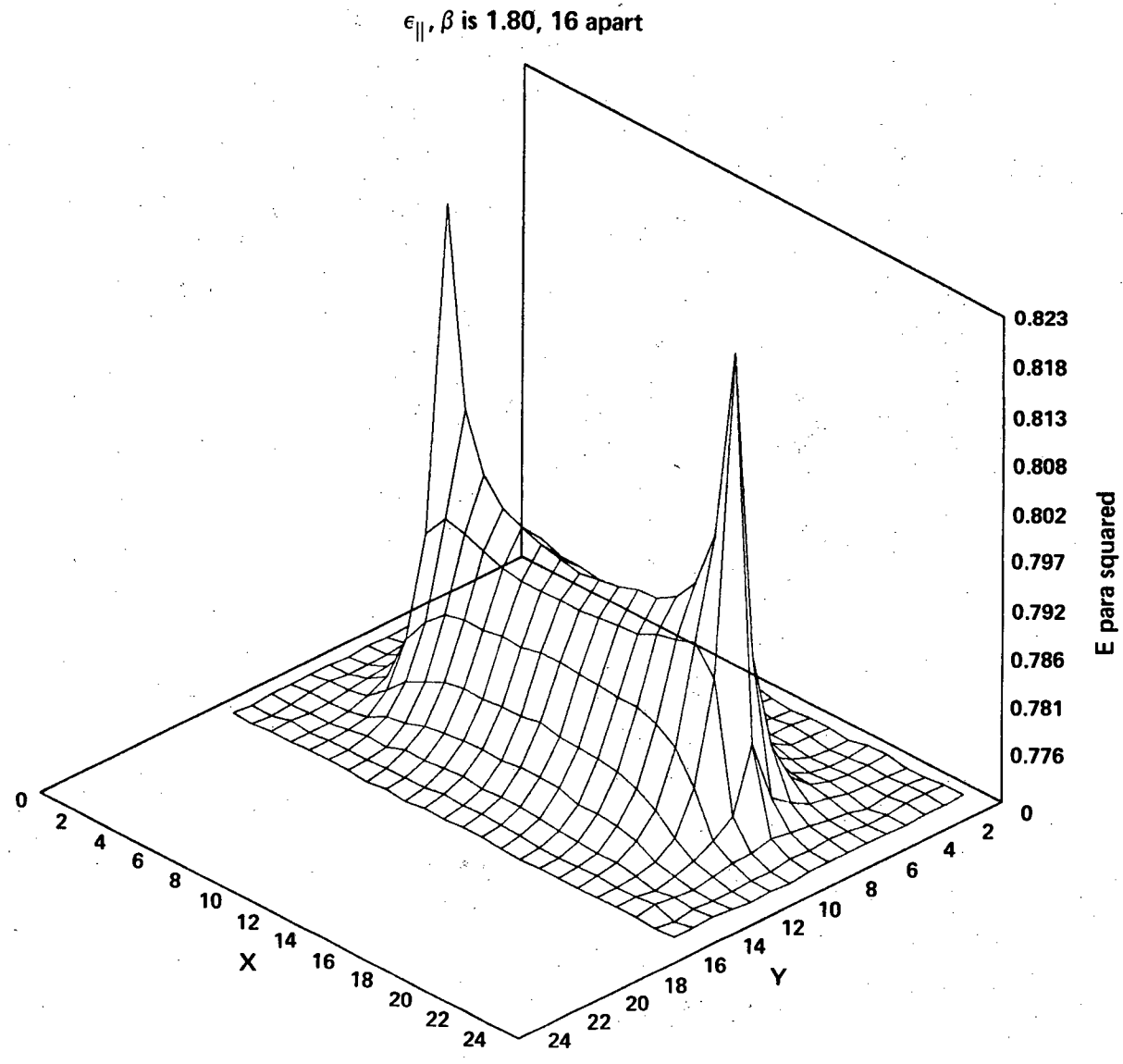

XBL-829-7281

FIGURE 5A

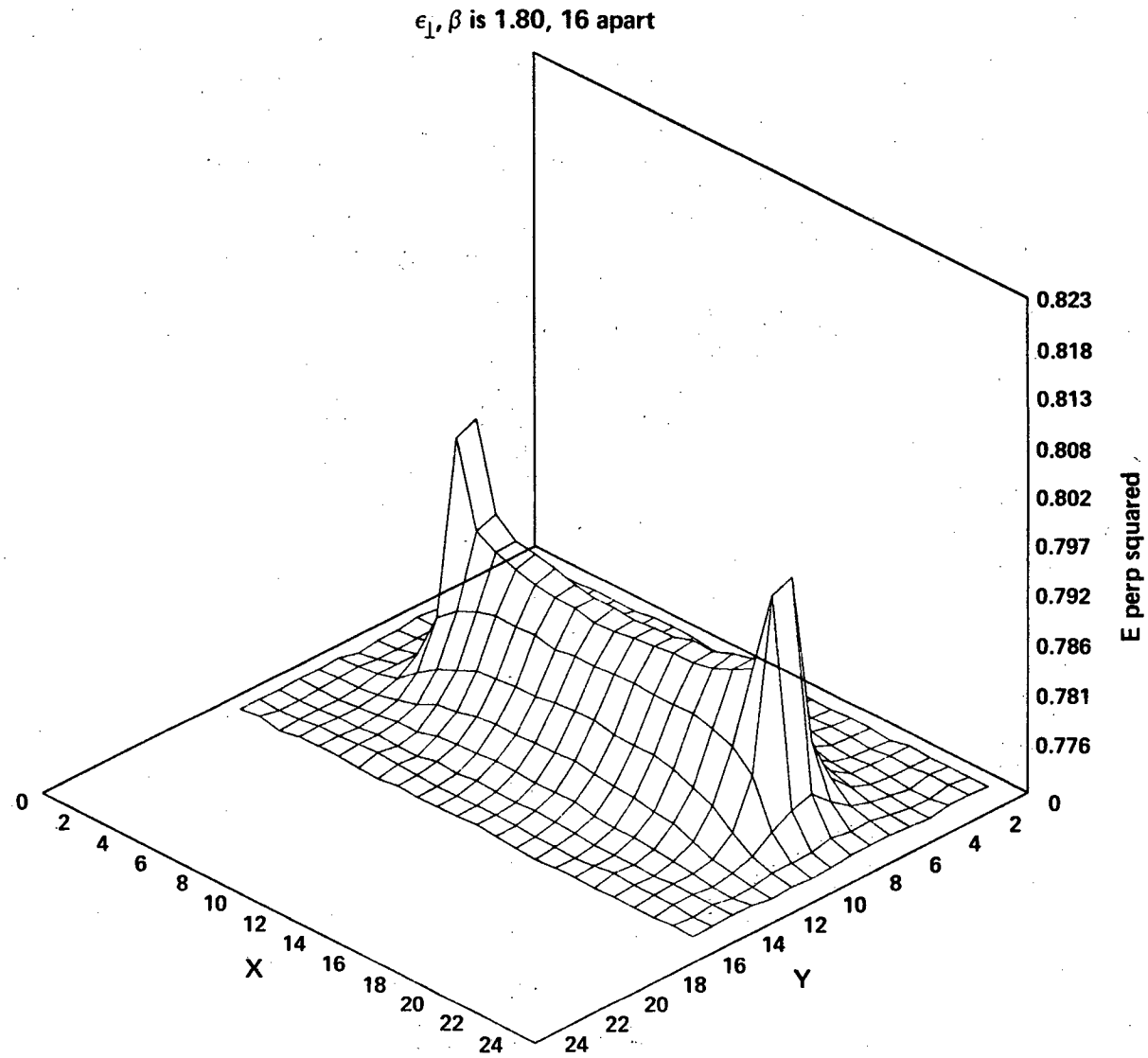
$\epsilon_\perp, \beta$ is 1.80, 16 apart
0.823
0.818
0.813
0.808
0.802
0.797
0.792
0.786
0.781
0.776
E perp squared
0
2
4
6
8
10
12
14
16
18
20
22
24
X
Y
XBL-829-7289

FIGURE 5B

ϵ_B, β is 1.80, 16 apart

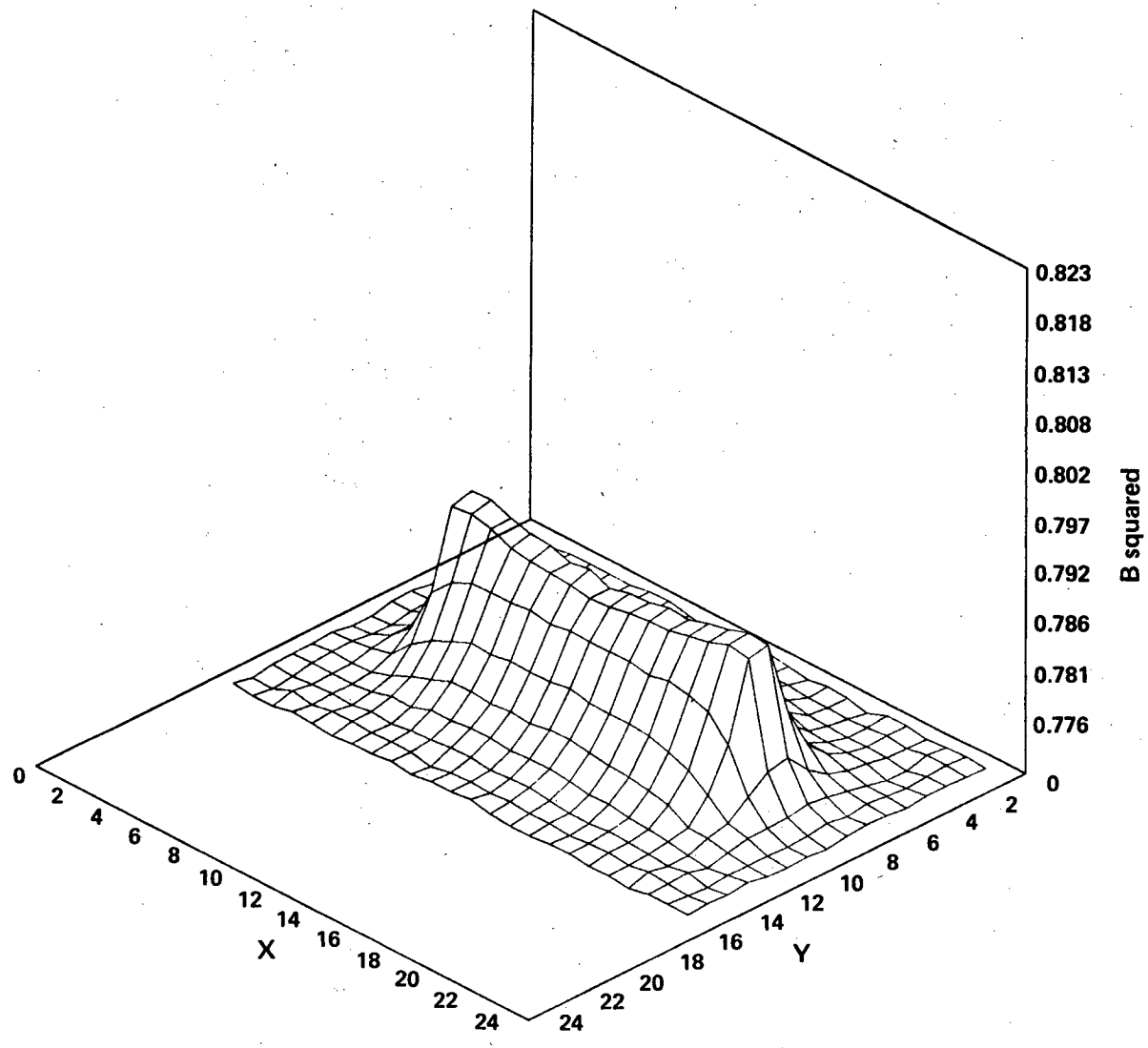

XBL-829-7277

FIGURE 5C

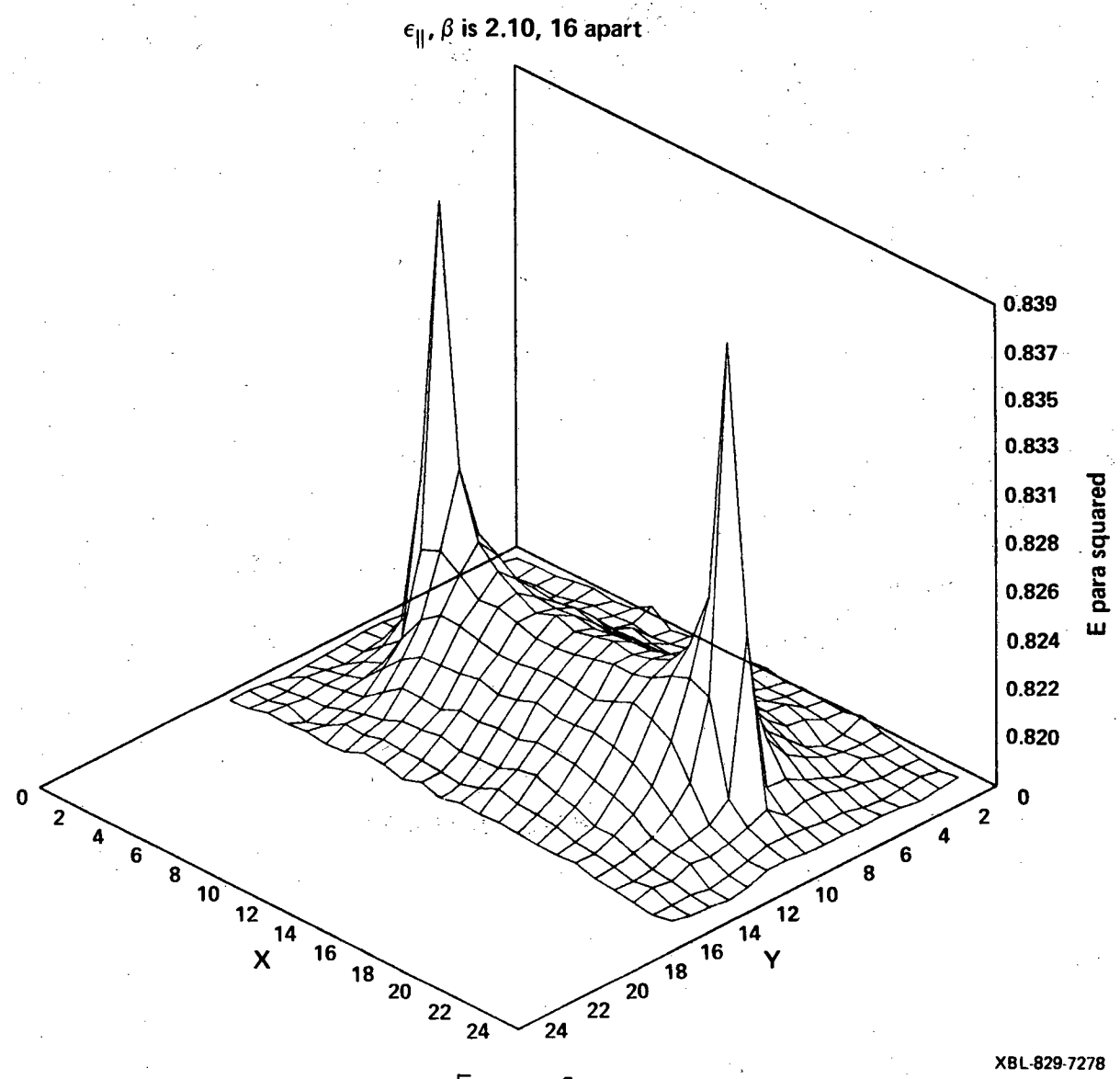
$\epsilon_{\|}$, β is 2.10, 16 apart
0.839
0.837
0.835
0.833
0.831
0.828
0.826
0.824
0.822
0.820
E para squared
0
2
4
6
8
10
12
14
16
18
20
22
24
X
Y
XBL-829-7278

FIGURE 6A

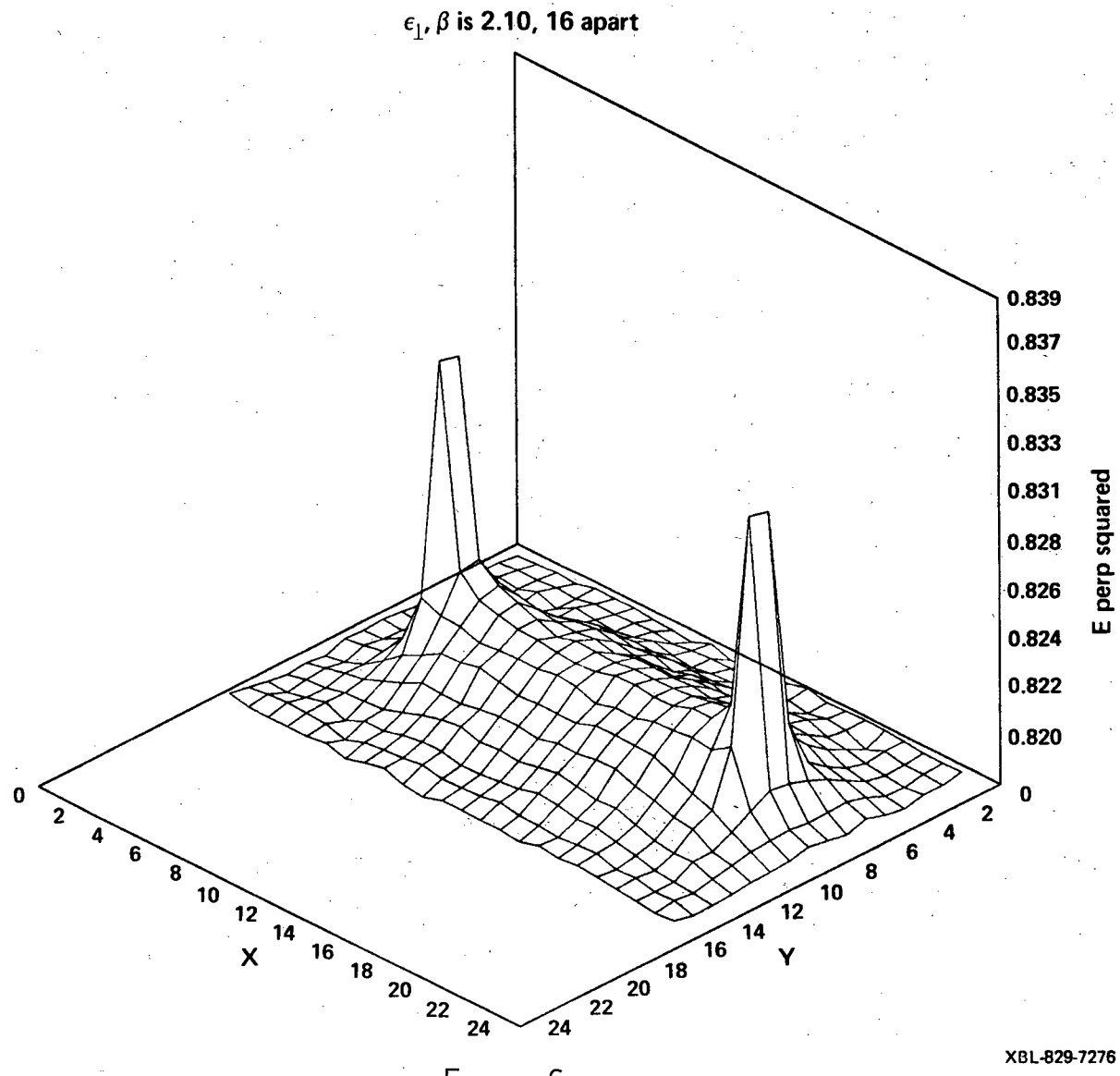
$\epsilon_\perp$, β is 2.10, 16 apart
0.839
0.837
0.835
0.833
0.831
0.828
0.826
0.824
0.822
0.820
0
E perp squared
0 2 4 6 8 10 12 14 16 18 20 22 24
X
0 2 4 6 8 10 12 14 16 18 20 22 24
Y
XBL-829-7276

FIGURE 6B

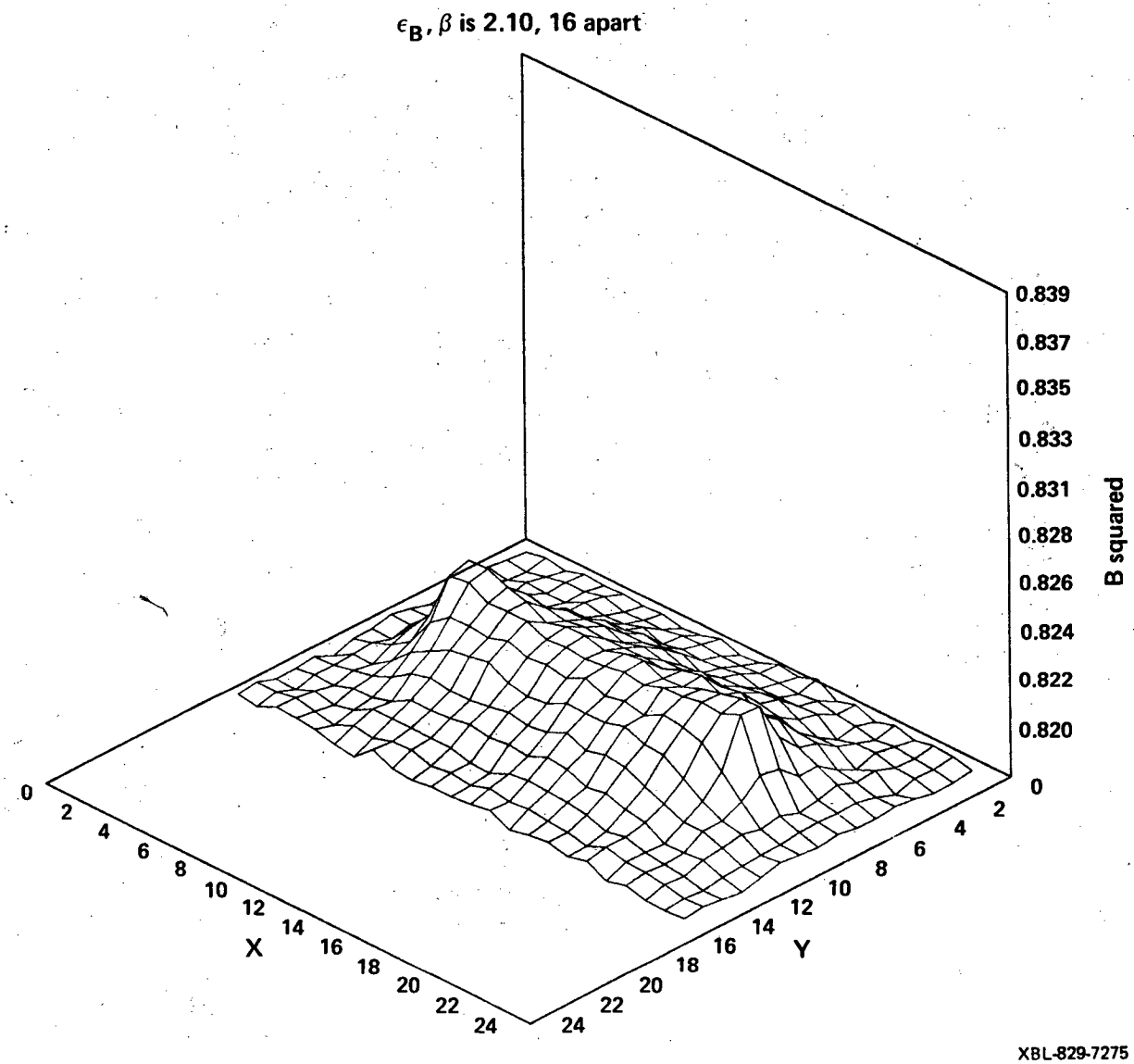

XBL-829-7275

FIGURE 6c

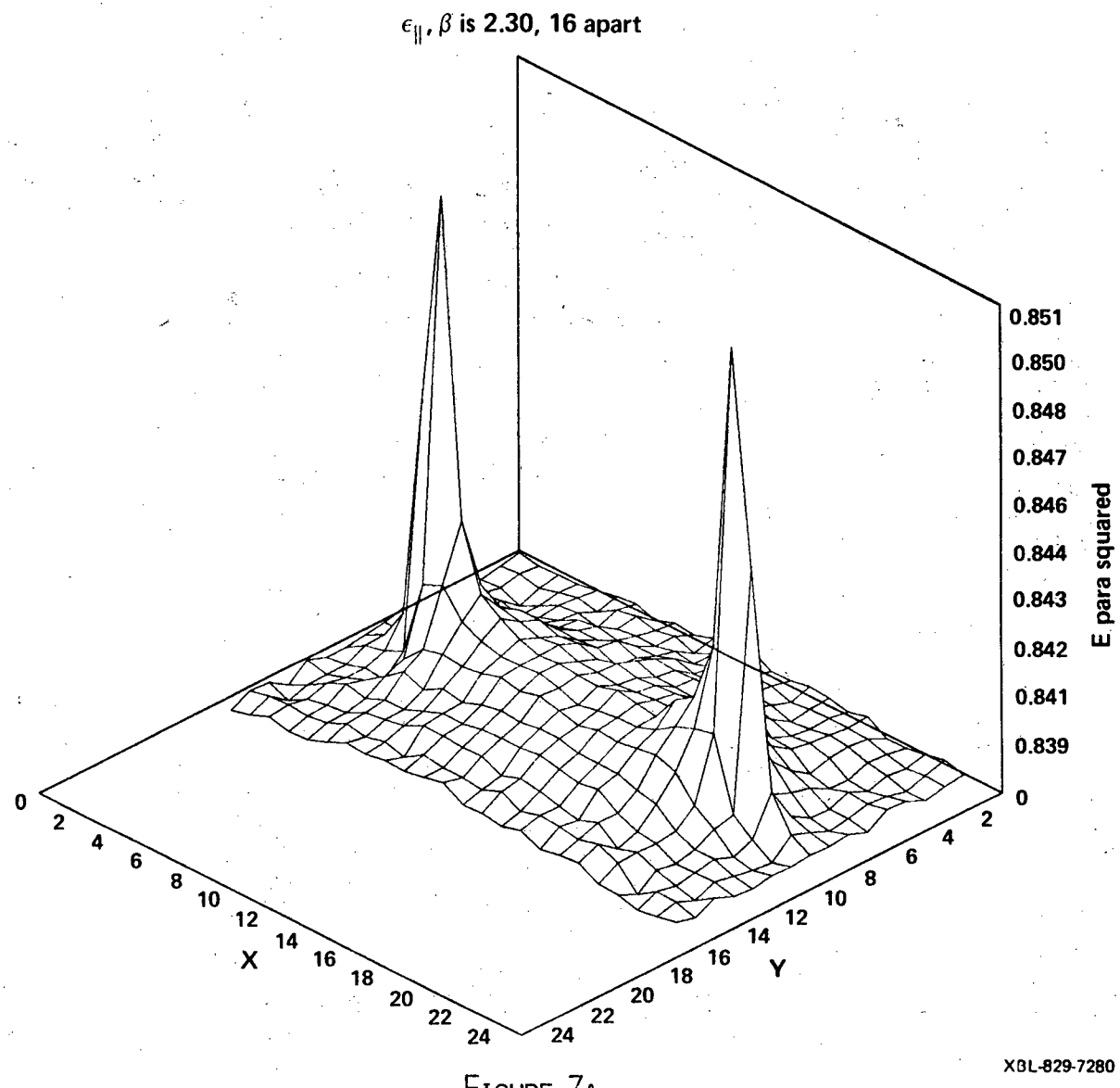

XBL-829-7280

FIGURE 7A

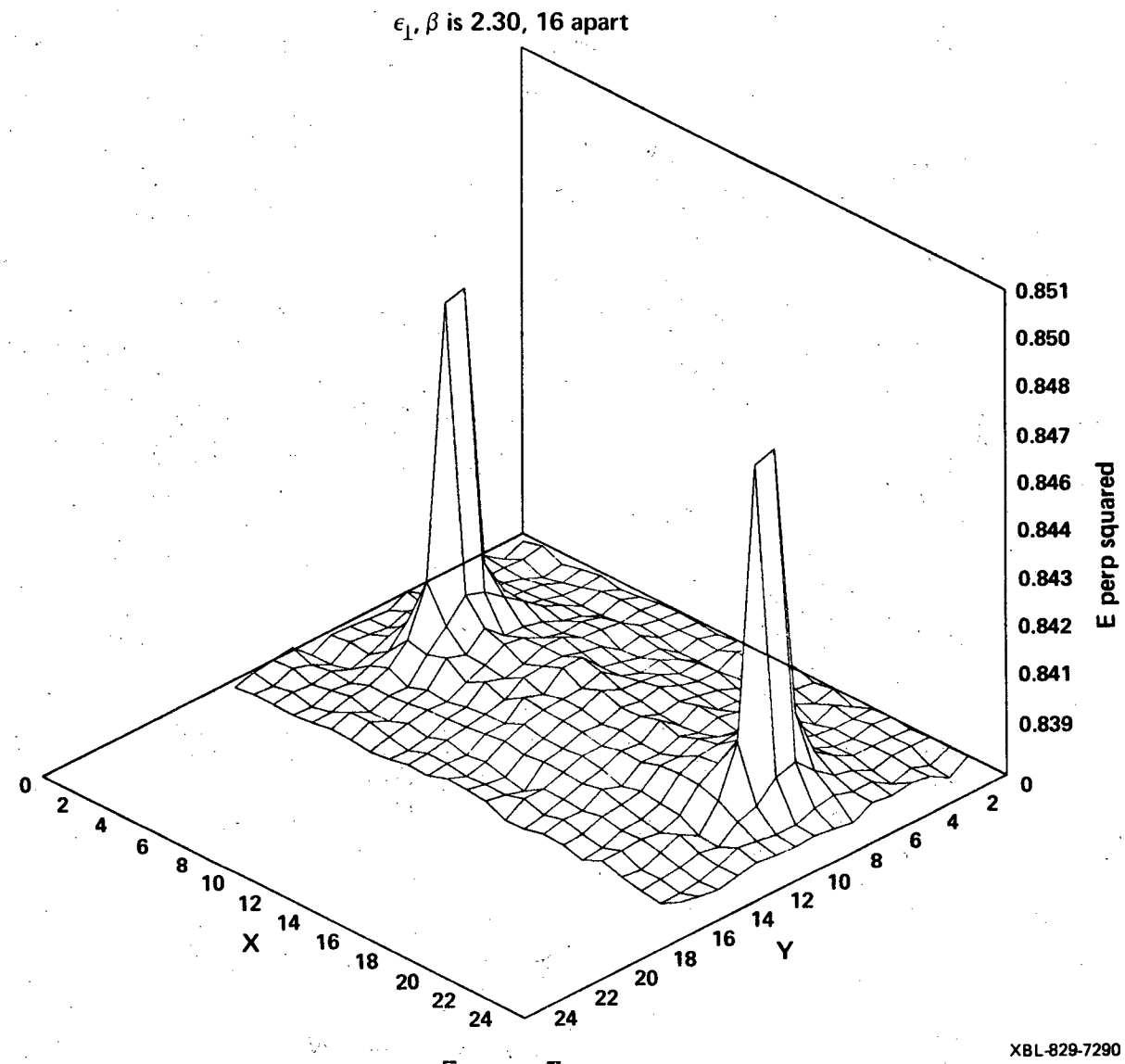
$\epsilon_\perp, \beta$ is 2.30, 16 apart
0.851
0.850
0.848
0.847
0.846
0.844
0.843
0.842
0.841
0.839
E perp squared
0
2
4
6
8
10
12
14
16
18
20
22
24
X
Y
XBL-829-7290

FIGURE 7B

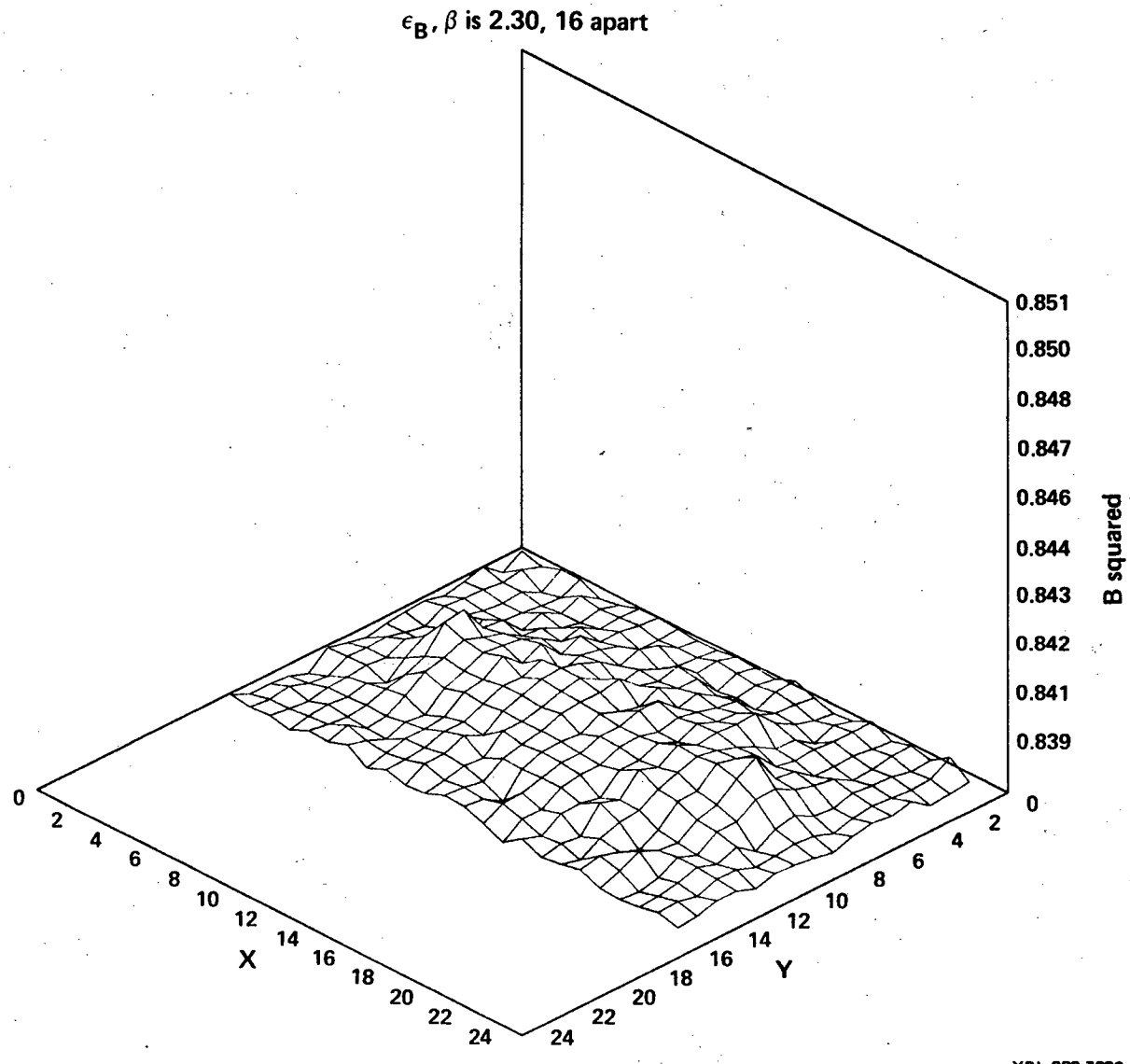

FIGURE 7c

XBL-829-7286

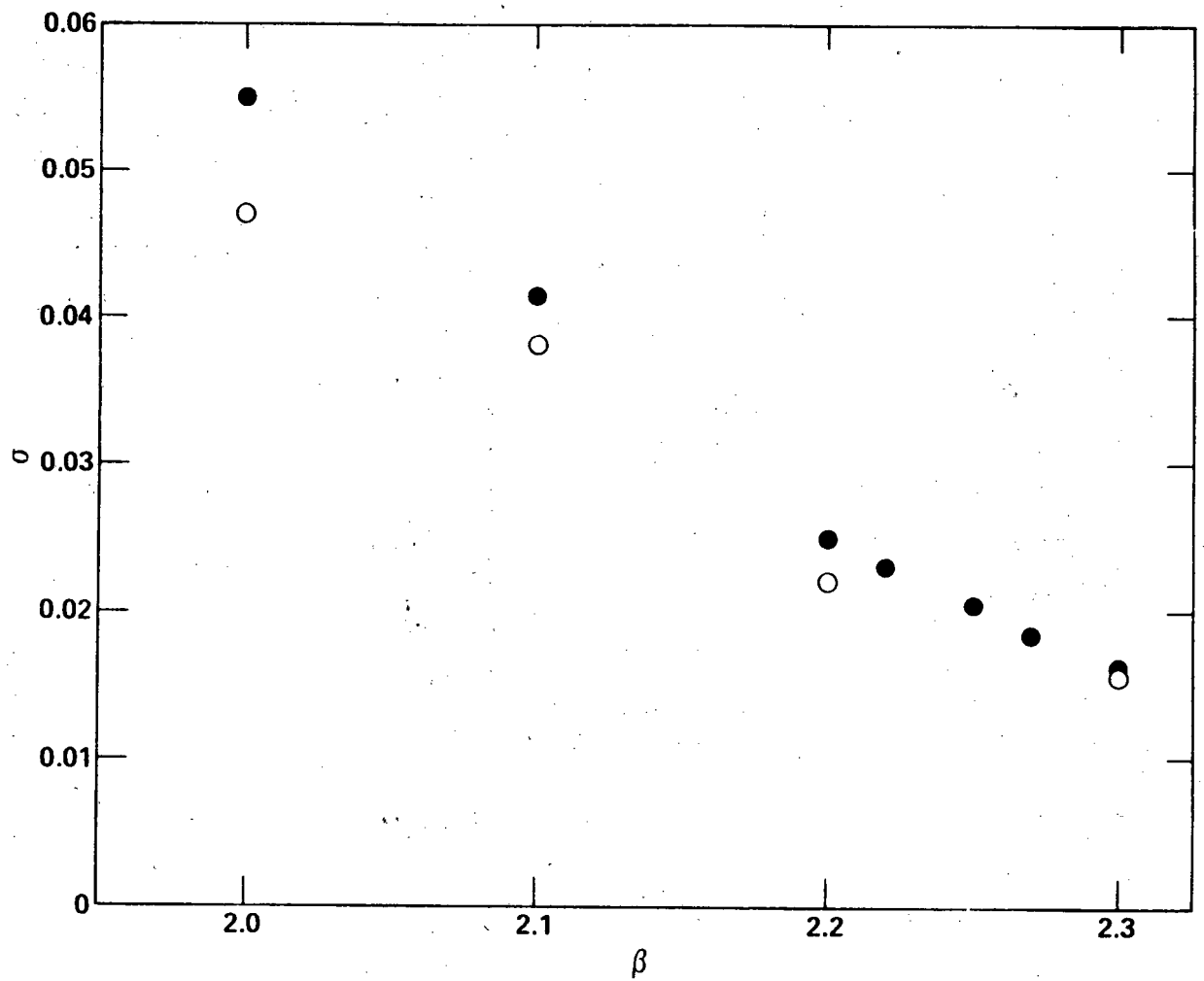

XBL-828-7264

FIGURE 8

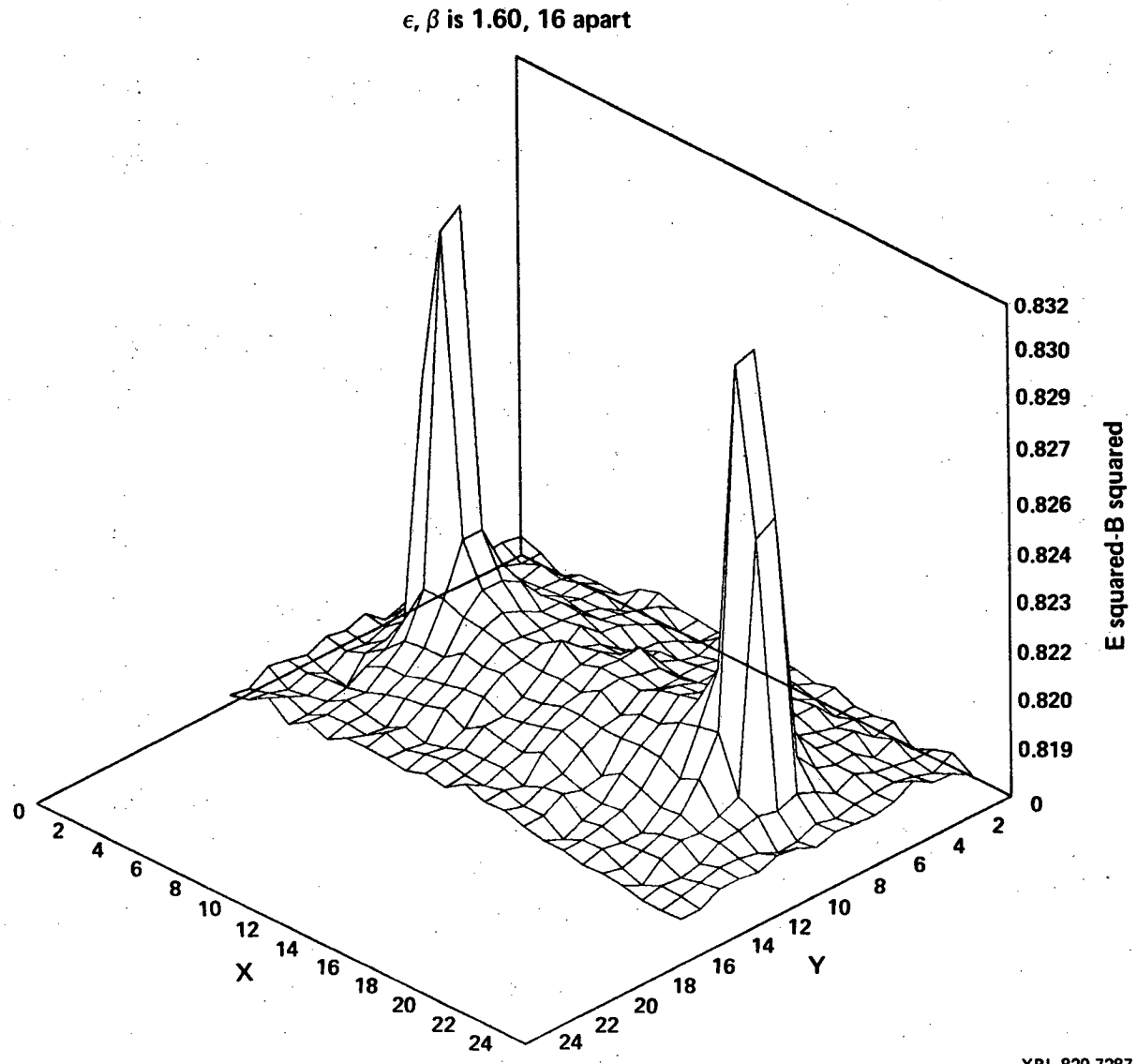
ε, β is 1.60, 16 apart
0.832
0.830
0.829
0.827
0.826
0.824
0.823
0.822
0.820
0.819
0
E squared-B squared
0
2
4
6
8
10
12
14
16
18
20
22
24
X
Y
XBL-829-7287

FIGURE 9A

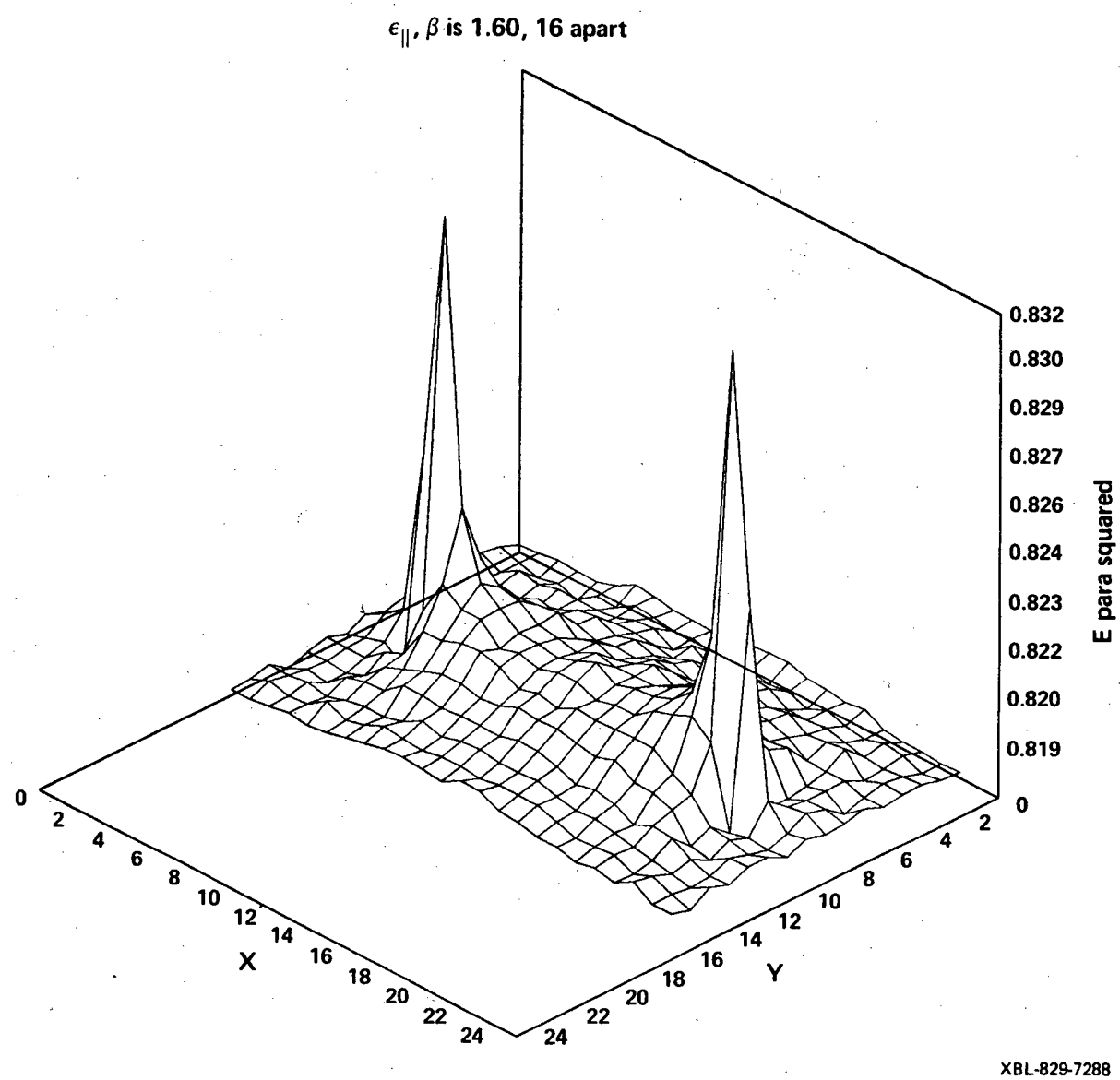
$\epsilon_{||}$, β is 1.60, 16 apart
0.832
0.830
0.829
0.827
0.826
0.824
0.823
0.822
0.820
0.819
E para squared
0
2
4
6
8
10
12
14
16
18
20
22
24
X
Y
XBL-829-7288

FIGURE 9B

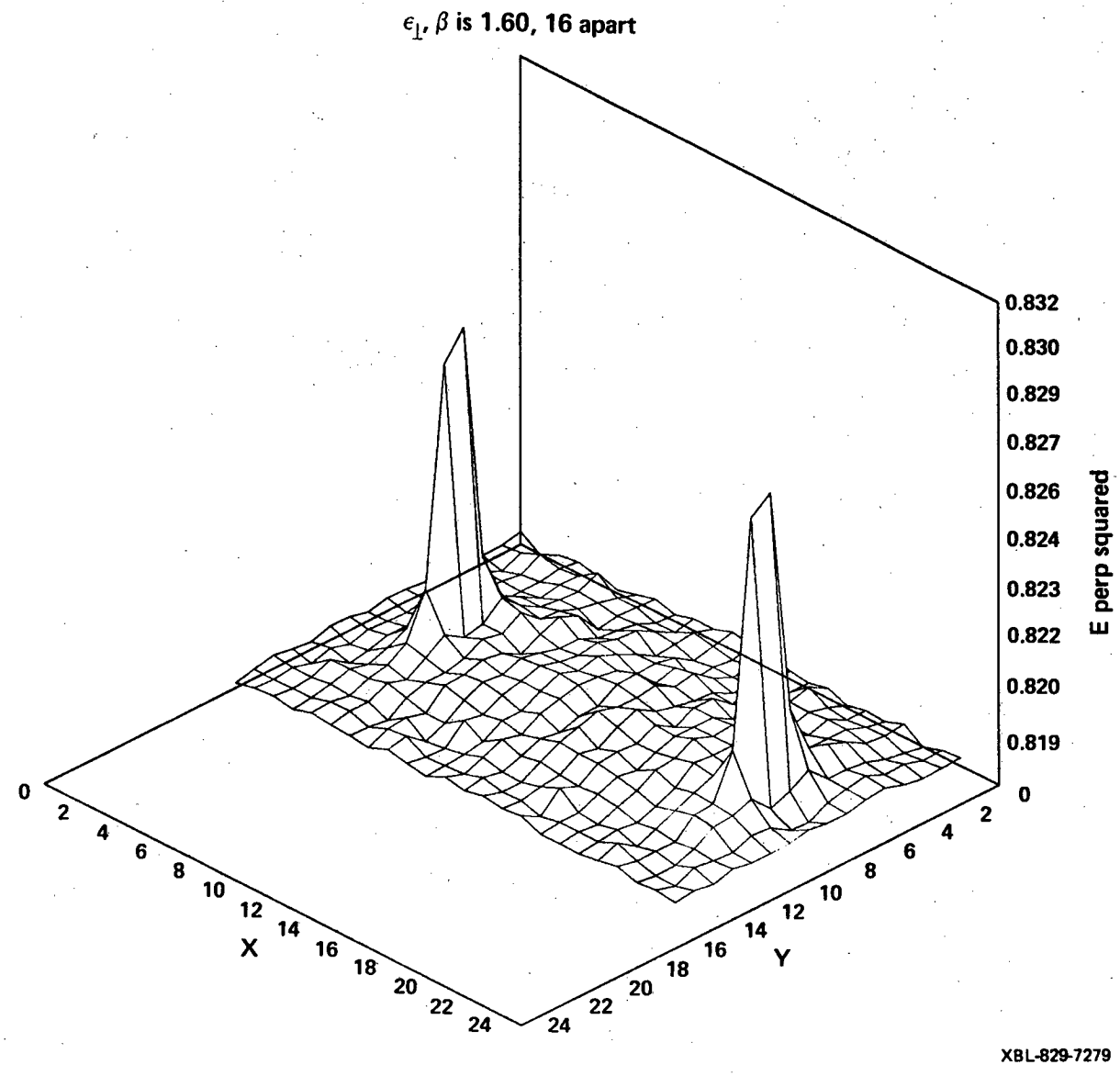
$\epsilon_\perp$, β is 1.60, 16 apart
0.832
0.830
0.829
0.827
0.826
0.824
0.823
0.822
0.820
0.819
0
E perp squared
0
2
4
6
8
10
12
14
16
18
20
22
24
X
Y
XBL-829-7279

FIGURE 9c

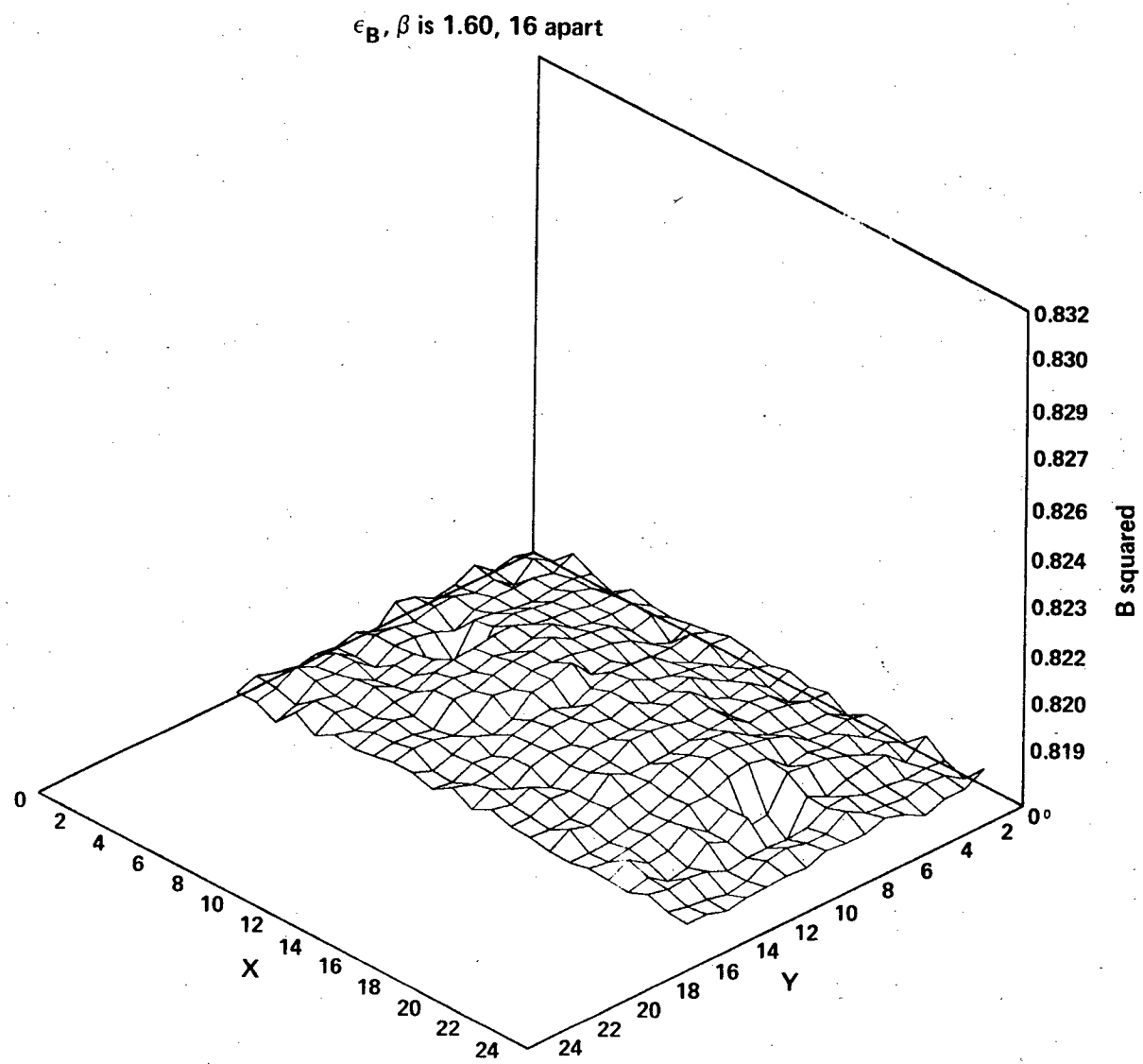

XBL-829-7285

FIGURE 9D

This report was done with support from the Department of Energy. Any conclusions or opinions expressed in this report represent solely those of the author(s) and not necessarily those of The Regents of the University of California, the Lawrence Berkeley Laboratory or the Department of Energy.

Reference to a company or product name does not imply approval or recommendation of the product by the University of California or the U.S. Department of Energy to the exclusion of others that may be suitable.

TECHNICAL INFORMATION DEPARTMENT
LAWRENCE BERKELEY LABORATORY
UNIVERSITY OF CALIFORNIA
BERKELEY, CALIFORNIA 94720